The Tungsten–Tungsten Triple Bond. 13.[1] Bisalkyl Tetracarboxylates of Dimolybdenum and Ditungsten. Triple Bonds between Metal Atoms with the Valence Molecular Orbital Description $\pi^4\delta^2$

Malcolm H. Chisholm,*[1a] David L. Clark,[1b] John C. Huffman,[1a] William G. Van Der Sluys,[1a] Edward M. Kober,[1c] Dennis L. Lichtenberger,[1c] and Bruce E. Bursten[1d]

Contribution from the Department of Chemistry and Molecular Structure Center, Indiana University, Bloomington, Indiana 47405, the Department of Chemistry, University of Arizona, Tucson, Arizona 85721, and the Department of Chemistry, The Ohio State University, Columbus, Ohio 43210. Received November 25, 1986

Abstract: Four synthetic procedures have been developed for the preparation of compounds of formula $W_2R_2(O_2CR')_4$: (1) $W_2R_2(NMe_2)_4 + 4R'COOCOR' \rightarrow W_2R_2(O_2CR')_4 + 4R'CONMe_2$; (2) $W_2R_2(OR'')_4 + 4R'COOH \rightarrow W_2R_2(O_2CR')_4 + 4R''OH$; (3) $W_2R_2(O_2CR')_4 + 4R''COOH \rightarrow W_2R_2(O_2CR'')_4 + 4R'COOH$; (4) $W_2R_6 + 4R'COOH \rightarrow W_2R_2(O_2CR')_4 + 4RH$. In all but one case (R = i-Bu) the R group lacks β-hydrogen atoms, and representative combinations of R = Me, Ph, Bz (benzyl), p-tolyl, o-tolyl, np (np = neopentyl), and CH_2SiMe_3 with R' = H, Me, CF_3, Et, Ph, p-MeOPh, t-Bu, mesityl, and $CHPh_2$ have been obtained by reactions in hydrocarbon or CH_2Cl_2 solvents at or below room temperature. Reaction 1 has been most extensively employed and has been extended to the synthesis of $Mo_2(np)_2(O_2CMe)_4$. Limiting factors to the generalized syntheses of $M_2R_2(O_2CR')_4$ compounds involve the ease of reductive elimination from the M_2^{6+} center, which occurs more readily (i) for M = Mo than M = W and (ii) for R = a β-hydrogen-containing alkyl ligand relative to a β-hydrogen-lacking (stabilized) ligand. In the case of the latter, reductive elimination is still possible by M–C bond homolysis, which may be thermally or photochemically induced. Photolysis allows for the generalized syntheses of $W_2(O_2CR')_4$ (M$\overset{4}{-}$M) compounds, including the formate, which has not previously been obtained by alternate methods. The compounds of formula $M_2R_2(O_2CR')_4$ have been characterized by IR spectroscopy, mass spectroscopy, NMR studies, cyclic voltammetry, UV–visible spectroscopy, and photoelectron spectroscopy, and, in certain cases, single-crystal X-ray studies have been carried out: M = Mo, R = np, R' = Me; M = W, (i) R = Bz, R' = Et; (ii) R = np, R' = Et; (iii) R = np, R' = Ph; (iv) R = np, R' = H; (v) R = np, R' = Me and CF_3, viz., $W_2(np)_2(O_2CMe)_2(O_2CCF_3)_2$. In the solid state all of the structurally characterized compounds have a central $M_2(O_2C)_4$ paddle-wheel core, typical of $M_2(O_2CR')_4$ compounds with M–M quadruple bonds, supplemented by axially aligned M–C(alkyl/aryl) bonds. Of particular note is the fact that the W–W distances in $W_2R_2(O_2CR')_4$ compounds, 2.18–2.20 Å, are essentially identical with those in the d^4–d^4 $W_2(O_2CR')_4$ compounds while the W–C bonds are as expected, ca. 2.17–2.21 Å. The Mo–Mo distance in $Mo_2(np)_2(O_2CMe)_4$, 2.13 Å, is longer by 0.04 Å than that found in $Mo_2(O_2CMe)_4$ (M$\overset{4}{-}$M). The M–O distances are essentially identical in the d^3–d^3 and d^4–d^4 compounds, ca. 2.08 Å. The M–M distances in the new compounds are the shortest thus far reported for d^3–d^3 dinuclear compounds of tungsten and molybdenum. In general, the ^{1}H NMR studies indicate the geometry found in the solid-state is maintained in solution but, for less bulky combinations of R and R', an alternate isomer is present; e.g., $W_2Me_2(O_2CMe)_4$ is spectroscopically analogous to $W_2Me_2(O_2CNEt_2)_4$, which has equatorially aligned W–C bonds with a C_{2v}-$W_2C_2(O_2C)_4$ core. For $W_2Bz_2(O_2CEt)_4$ a mixture of the two isomers is present in solution and the equilibrium constant is solvent dependent: the relative concentration of the C_{2v}- to D_{4h}-$W_2C_2(O_2C)_4$ isomer is ca. 1:2 in CD_2Cl_2 and ca. 1:8 in toluene-d_8 and benzene-d_6. Spectroscopic studies on the axially ligated compounds $W_2R_2(O_2CR')_4$ indicate that the valence M–M MO description is $\pi^4\delta^2$, i.e., directly analogous to that of the $M_2(O_2CR')_4$ compounds except with respect to the presence of the M–M σ bond. This conclusion is reached by a comparison of the photoelectron spectra, the UV–visible spectra, and cyclic voltammetric studies. An assignment of the $^1(\delta \rightarrow \delta^*)$ transition is possible for both the d^3–d^3 and d^4–d^4 compounds, and the effect of conjugation of aromatic rings on the $\delta \rightarrow \pi^*_{(oco)}$ MLCT transition is experimentally and theoretically clarified with respect to earlier studies on $W_2(O_2CAr)_4$ (M$\overset{4}{-}$M) compounds. In the photoelectron spectra an ionization from one of the M–C σ bonds is close in energy to the ionization from the M–M π bonds. The M–M bonds of valence MO configuration $\pi^4\delta^2$ are remarkably short in terms of the simplistic view that occupation of M–M σ and σ* orbitals effectively leads to a cancellation of σ-bonding contributions, e.g., as in He_2, $1\sigma^2 1\sigma^{*2}$. This is not the case in $M_2R_2(O_2CR')_4$ compounds because M–C and M–M σ and σ* mixing occurs such that there is residual M–M σ bonding in the d^3–d^3 dinuclear compounds. The magnitude of this residual M–M σ bonding is greater for M = W than M = Mo because of relativistic effects. This is the first recognition of this phenomenon for M–M multiple bonds, and a comparison with the bonding in the diatomic molecule C_2 and that in HC≡CH is noted. Formally C_2 has the MO configuration $1\sigma^2 1\sigma^{*2} 2\sigma^2 2\sigma^{*2} 1\pi^4$, i.e., a net double bond lacking a σ component, but s–p mixing effectively increases the bonding in 2σ and decreases the antibonding in $2\sigma^*$. In the $M_2(O_2CR')_4$ compounds there are two significant MOs having M–M σ character because of valence s and d_{z^2} mixing. The bonding in the R–E≡E–R units in acetylene (E = C) and in $E_2R_2(O_2CR')_4$ compounds (E = Mo, W) has extensive mixing of E–R and E–E σ and σ* orbitals. The spectroscopic results are compared to a previous Xα–SW calculation [*J. Am. Chem. Soc.* **1985**, *107*, 4459].

The tetracarboxylates of dimolybdenum and ditungsten are among the best known of the compounds containing quadruple bonds, $\sigma^2\pi^4\delta^2$, between metal atoms.[2] The formation of $Mo_2(O_2CR)_4$ compounds in the reactions between $Mo(CO)_6$ and RCOOH has provided an easy entry into the chemistry of the Mo_2^{4+} unit.[2-7] Though analogous reactions involving $W(CO)_6$

(1) For part 12 in the series see: Chisholm, M. H.; Chiu, H. T.; Huffman, J. C.; Wang, R. *Inorg. Chem.* **1986**, *25*, 1092. (a) Indiana University. (b) 1985–1986 Indiana University General Electric Fellow. (c) University of Arizona. (d) The Ohio State University.

(2) Cotton, F. A.; Walton, R. A. *Multiple Bonds between Metal Atoms*; Wiley: New York, 1982.
(3) Abel, E. W.; Singh, A.; Wilkinson, G. *J. Chem. Soc.* **1959**, 3097.
(4) Stephenson, T. A.; Bannister, E.; Wilkinson, G. *J. Chem. Soc.* **1964**, 2538.
(5) Holste, G.; Schafer, H. *Z. Anorg. Allg. Chem.* **1972**, *391*, 263.

have long been studied,[8-10] only within the past few years have $W_2(O_2CR)_4$ compounds been prepared, and then only by alternate routes that prevent oxidation of the ditungsten center.[11,12]

The structural signature of the $M_2(O_2CR)_4$ compounds is the four-bladed paddle wheel with short M–M distances, ca. 2.10 Å for M = Mo[13-16] and 2.20 Å for M = W.[12] These compounds have been the subject of numerous spectroscopic studies. Although not without initial controversy,[17-20] certain of the electronic absorptions in their UV–visible spectra can now reliably be established as $\delta \rightarrow \delta^*$ and $\delta \rightarrow CO_2\pi^*$.[21,22] Again in the photoelectron spectra[15,23,24] the lowest energy ionizations, corresponding to the highest energy MOs, follow the order, M–M δ, π, and σ, though the location and the significance of the ionization from the M–M σ orbital have only recently been realized.[25-27] The $M_2(O_2CR)_4$ compounds also show reversible electrochemical oxidations in cyclic voltammetry, and the influence of the substituents on the carboxylate as well as the metal, Mo vs. W, can be correlated with data from photoelectron spectroscopic studies.[22,28,29]

In this paper we describe the synthesis and characterization of a new series of compounds of formula $M_2R_2(O_2CR')_4$. These adopt structures closely related to those of the dimetal tetracarboxylates having axially aligned alkyl ligands as diagrammatically shown in I.[30,31]
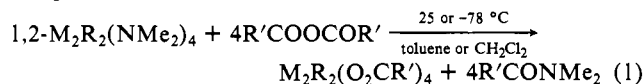

I
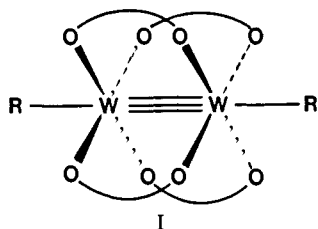
(6) Hochberg, E.; Walks, P.; Abbott, E. H. *Inorg. Chem.* 1974, *13*, 1824.

(7) Brignole, A. B.; Cotton, F. A. *Inorg. Synth.* 1972, *13*, 81.

(8) Stephenson, T. A.; Whittaker, D. *Inorg. Nucl. Chem. Lett.* 1969, *5*, 569.

(9) Cotton, F. A.; Jeremic, M. *Synth. Inorg. Met. Org. Chem.* 1971, *1*, 265.

(10) Holste, G. *Z. Anorg. Allg. Chem.* 1973, *398*, 249.

(11) Sattelberger, A. P.; McLaughlin, K. W.; Huffman, J. C. *J. Am. Chem. Soc.* 1981, *103*, 2880.

(12) Santure, D. J.; McLaughlin, K. W.; Huffman, J. C.; Sattelberger, A. P. *Inorg. Chem.* 1983, *22*, 1877.

(13) Cotton, F. A.; Mester, Z. C.; Webb, T. R. *Acta Crystallogr., Sect. B.* 1974, *B30*, 2768.

(14) Cotton, F. A.; Norman, J. G., Jr. *J. Coord. Chem.* 1972, *1*, 161.

(15) Cotton, F. A.; Norman, J. G., Jr.; Stults, B. R.; Webb, T. R. *J. Coord. Chem.* 1976, *5*, 217.

(16) Cotton, F. A.; Extine, M. W.; Gage, L. D. *Inorg. Chem.* 1978, *17*, 172.

(17) Norman, J. G., Jr.; Kolari, H. J.; Gray, H. B.; Trogler, W. C. *Inorg. Chem.* 1977, *16*, 987.

(18) Cotton, F. A.; Martin, D. S.; Fanwick, P. E.; Peters, T. J.; Webb, T. R. *J. Am. Chem. Soc.* 1976, *98*, 4681.

(19) Cotton, F. A.; Martin, D. S.; Webb, T. R.; Peters, T. J. *Inorg. Chem.* 1976, *15*, 1199.

(20) Trogler, W. C.; Solomon, E. I.; Trabjerg, I.; Ballhausen, C. J.; Gray, H. B. *Inorg. Chem.* 1977, *16*, 828.

(21) Martin, D. S.; Newman, R. A.; Fanwick, P. E. *Inorg. Chem.* 1979, *18*, 2511.

(22) Santure, D. J.; Huffman, J. C.; Sattelberger, A. P. *Inorg. Chem.* 1985, *24*, 371.

(23) Coleman, A. W.; Green, J. C.; Hayes, A. J.; Seddon, E. A.; Lloyd, D. R.; Niwa, Y. *J. Chem. Soc., Dalton Trans.* 1979, 1057.

(24) Green, J. C.; Hayes, A. J. *Chem. Phys. Lett.* 1975, *31*, 306.

(25) Bancroft, G. M.; Pellach, E.; Sattelberger, A. P.; McLaughlin, K. W. *J. Chem. Soc., Chem. Commun.* 1982, 752.

(26) Green and co-workers[24] had actually suggested that the Mo–Mo σ ionization in $Mo_2(O_2CR)_4$ compounds may well be found under the π ionization. That notion was not fully considered at the time since it was not consistent with expectations based upon Xα–SW results.

(27) Kober, E. M.; Lichtenberger, D. L. *J. Am. Chem. Soc.* 1985, *107*, 7199.

(28) Bursten, B. E.; Cotton, F. A.; Cowley, A. M.; Hanson, B. E.; Lattman, M.; Stanley, G. G. *J. Am. Chem. Soc.* 1979, *101*, 6244.

(29) Cotton, F. A.; Pederson, E. *Inorg. Chem.* 1975, *14*, 399.

(30) Chisholm, M. H.; Hoffman, D. M.; Huffman, J. C.; Van Der Sluys, W. G.; Russo, S. *J. Am. Chem. Soc.* 1984, *106*, 5386.

Of particular note in this series are the M–M distances, which are the shortest known for M_2^{6+}-containing compounds of molybdenum[31] and tungsten.[30] We show, beyond a reasonable doubt, that the valence MO description for the $(M\equiv M)^{6+}$ unit is $\pi^4\delta^2$. This work adds a new chapter to the chemistry of multiple bonds between metal atoms and provides insight into the interpretations of several longstanding problems.
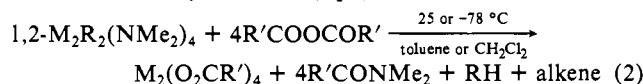
Results and Discussion

Syntheses. Four routes have been employed for the syntheses of the new compounds. The most extensively studied is shown in eq 1.

$$1,2\text{-}M_2R_2(NMe_2)_4 + 4R'COOCOR' \xrightarrow[\text{toluene or } CH_2Cl_2]{25 \text{ or } -78 \text{ °C}}$$
$$M_2R_2(O_2CR')_4 + 4R'CONMe_2 \quad (1)$$

There are certain general limitations to the success of reaction 1:

(1) When R is an alkyl group containing β-hydrogen atoms, reductive elimination by alkyl group disproportionation is generally, but not universally, observed (eq 2).[32]

$$1,2\text{-}M_2R_2(NMe_2)_4 + 4R'COOCOR' \xrightarrow[\text{toluene or } CH_2Cl_2]{25 \text{ or } -78 \text{ °C}}$$
$$M_2(O_2CR')_4 + 4R'CONMe_2 + RH + \text{alkene} \quad (2)$$

The facile reductive elimination in eq 2 has allowed a general route to $W_2(O_2CR')_4$ compounds.[33] However, in the case of R = *i*-Bu, it is possible to prepare the $M_2(i\text{-}Bu)_2(O_2CR')_4$ compounds at low temperatures, and, once formed, the alkyl–tungsten bond is thermally quite resistant to reductive elimination by β-hydrogen abstraction mechanisms. This finding may be understood in terms of the facts that (i) the *i*-Bu ligand has only one β-hydrogen atom, (ii) once the $M_2(i\text{-}Bu)_2(O_2CR')_4$ compounds are formed having a structure of type I, there are no available metal orbitals for M–H–C interactions, thus shutting off the four-center mechanism for β-hydrogen elimination, and (iii) during the course of the R'COO for NMe$_2$ substitution, the intermediates of formula $M_2(i\text{-}Bu)_2(O_2CR')_x(NMe_2)_{4-x}$ probably have a conformationally stabilized β-hydrogen atom in the *i*-Bu ligand. The preferred M–C–C–H conformation is probably anti, with the CMe$_2$ groups being distal to the W–W bond, as seen in the molecular structure of $W_2(i\text{-}Bu)_2(O\text{-}i\text{-}Pr)_4$.[34]

(2) A second limitation to the success of eq 1 involves metal–carbon bond homolysis reactions. This again leads to $M_2(O_2CR')_4$ compounds, and the organic radical R· can either couple or abstract H· from the solvent (or D· in deuteriated solvents). The inertness of the M–C bond follows the order W > Mo and np (neopentyl) > Me > Bz (benzyl) > aryl. The only compounds isolated and fully characterized for molybdenum involve the neopentyl ligand.

(3) The other limitations to the success of eq 1 involve (i) the practicalities of separating the inorganic compound from the amide R'CONMe$_2$, which is often relatively nonvolatile and (ii) the ready availability of the acid anhydride.

It appears that compounds where R = np are easier to prepare than where R = Me, though once formed the methyl derivatives are equally stable. Steric factors may well be responsible for protecting the metal–carbon bond during the course of the reaction (reaction 1) though this matter is not understood.

The limitations to the preparation of $W_2R_2(O_2CR')_4$ compounds noted in (3) can sometimes be overcome by employing one of alternate synthetic routes. First, it is possible to carry out carboxylate ligand exchange reactions of the type shown in eq 3.

$$W_2R_2(O_2CR')_4 + 4R''COOH \xrightarrow[CH_2Cl_2]{25 \text{ °C}}$$
$$W_2R_2(O_2CR'')_4 + 4R'COOH \quad (3)$$
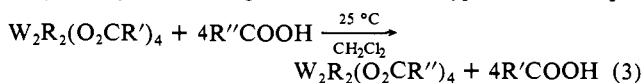
(31) Chisholm, M. H.; Huffman, J. C.; Van Der Sluys, W. G. *Inorg. Chim. Acta* 1986, *116*, L13.

(32) Chisholm, M. H.; Chiu, H. T., results to be published.

(33) Chisholm, M. H.; Chiu, H. T.; Huffman, J. C. *Polyhedron* 1984, *6*, 759.

(34) Chisholm, M. H.; Eichhorn, B. W.; Folting, K.; Huffman, J. C.; Tatz, R. J. *Organometallics* 1986, *5*, 1599.

Table I. Characterization Data for Compounds of the Formula $M_2R_2(O_2CR')_4$

compd	color	sublimation[a]	solution structure[b]	anal. (calcd/obsd)			
				% C	% H	% N	% F
$W_2Bz_2(O_2CEt)_4$	orange plates	decomp	I and II	37.09/37.68	4.04/4.21	0.00/<0.03	
$W_2Bz_2(O_2CMe)_4$	orange plates	decomp	I and II				
$W_2Bz_2(O_2CH)_4$	yellow powder	decomp	I and II				
$W_2Bz_2(O_2CCMe_3)_4$	orange plates	decomp	I				
$W_2Bz_2(O_2CPh)_4$	orange-red powder	decomp	I				
$W_2(o\text{-}MeC_6H_4)_2(O_2CEt)_4$	yellow powder	decomp	I and II	36.89/36.83	4.54/3.95	0.00/0.06	
$W_2(p\text{-}MeC_6H_4)_2(O_2CEt)_4$	yellow powder	decomp	I and II				
$W_2Me_2(O_2CPh)_4$	orange powder	>200 °C	I	40.84/40.62	6.02/5.93	0.00/0.06	
$W_2Me_2(O_2CMe)_4$	beige powder		II				
$W_2(CH_2CHMe_2)_2(O_2CMe)_4$	yellow-green powder	100–120 °C	I				
$W_2(CH_2CHMe_2)_2(O_2CPh)_4$	green-red needles		I				
$W_2(CH_2SiMe_3)_2(O_2CMe)_4$	green plates	decomp	I	26.61/24.59	4.75/4.25	0.00/0.07	
$W_2(np)_2(O_2CH)_4$	green cubes	100–120 °C	I	24.40/24.49	3.66/3.76	0.00/<0.03	
$W_2(np)_2(O_2CMe)_4$	green needles	120–130 °C	I	28.97/28.89	4.60/4.53	0.00/<0.03	
$W_2(np)_2(O_2CEt)_4$	green needles	120–130 °C	I	33.41/32.74	5.31/5.19	0.00/<0.03	
$W_2(np)_2(O_2CCMe_3)_4$	green powder	120–130 °C	I				
$W_2(np)_2(OAc)_3(TFA)$	green cubes	120–130 °C	I				
$W_2(np)_2(OAc)_2(TFA)_2$	yellow-orange cubes	120–130 °C	I				
$W_2(np)_2(OAc)(TFA)_3$	orange cubes	120–130 °C	I				
$W_2(np)_2(TFA)_4$	red-orange cubes	100–120 °C	I	22.47/22.46	2.28/2.36	0.00/<0.03	23.69/23.5
$W_2(np)_2(O_2CPh)_4$	green-red cubes	>200 °C	I	45.89/45.70	4.27/4.11	0.00/0.03	
$W_2(np)_2(O_2CPhOMe)_4$	green-orange cubes	>200 °C	I	45.26/45.03	4.53/4.70	0.00/0.07	
$W_2(np)_2(O_2CCHPh_2)_4$	yellow powder		I				
$W_2(np)_2(O_2C\text{-}mesityl)_4$	green powder	>200 °C	I	51.64/51.56	5.73/5.63	0.00/<0.03	
$Mo_2(np)_2(O_2CMe)_4$	orange plates	100–110 °C	I	37.90/40.95	6.02/5.93	0.00/0.06	

[a] At 10^{-4} Torr.   [b] Determined by ^1H NMR.

Reaction 3 has been used to prepare the formate $W_2(np)_2$-$(O_2CH)_4$, thereby obviating the use of formic anhydride.[35] Furthermore, the substitution of an alkyl carboxylate by an aryl carboxylate is readily achieved. If the compound bearing the O_2CR'' ligands is much less soluble than the compound with the O_2CR' ligands, care must be taken that precipitation of W_2R_2-$(O_2CR'')_4$ does not occur with coprecipitation of partially substituted compounds. We have, however, made use of the stepwise substitution reaction in the preparation of the mixed carboxylate cis-$W_2(np)_2(O_2CMe)_2(O_2CCF_3)_2$, which was of interest for mechanistic and spectroscopic purposes. The substitution occurs in a cis-stepwise manner as expected from considerations of the trans effect of $MeCO_2^-$ and $CF_3CO_2^-$.[36]

The third reaction procedure involves the addition of the free acid (anhydrous) to dialkyl tetraalkoxides (eq 4).

$$1,2\text{-}W_2R_2(OR'')_4 + 4R'COOH \xrightarrow[\text{toluene}]{25 °C}$$
$$W_2R_2(O_2CR')_4 + 4R''OH \quad (4)$$
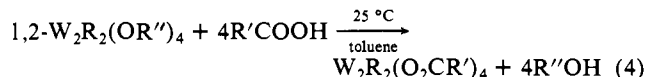
Studies of reaction 4 have not been extensive but it has the advantage that the alcohol and dimetal complex are readily separated. It has the disadvantage of having first to prepare the $1,2\text{-}W_2R_2(OR'')_4$ compound from $1,2\text{-}W_2R_2(NMe_2)_4$ and alcohol (4 equiv).[34]

A fourth reaction that produces $W_2R_2(O_2CR')_4$ compounds is outlined in eq 5.

$$W_2(np)_6 + 4CF_3CO_2H \xrightarrow[\text{toluene}]{25 °C} W_2(np)_2(O_2CCF_3)_4 + 4npH$$
$$(5)$$
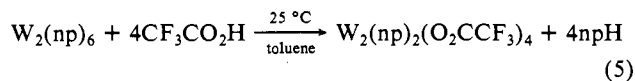
It was found by Wilkinson et al. that when $Mo_2(CH_2SiMe_3)_6$ was reacted with $MeCO_2H$, the quadruply bonded $Mo_2(O_2CMe)_4$ complex was formed.[37] We feel that $Mo_2(CH_2SiMe_3)_2(O_2CMe)_4$ is a likely intermediate in this reaction sequence. An obvious limitation to eq 5 is the paucity of W_2R_6 compounds.[37]

Finally, we note that the seemingly "obvious" route to $M_2R_2(O_2CR')_4$ compounds, involving the addition of the carboxylic acid $R'COOH$ to $1,2\text{-}M_2R_2(NMe_2)_4$ compounds just does not give

the desired products. The reasons for failure are not known, but the formation of salts, $Me_2NH_2^+O_2CR'^-$, could be responsible for the formation of different products.[38]

Physicochemical Properties. The new compounds are thermally stable at room temperature in the solid state. Several sublime when heated in vacuo without significant decomposition. Except for R = benzyl and aryl, the compounds are also stable in hydrocarbon and chlorinated organic solvents such as CH_2Cl_2 and $CHCl_3$. Elemental analyses and other characterization data are summarized in Table I.

The volatile compounds gave weak molecular ions in the mass spectrometer, $M_2R_2(O_2CR')_4^+$, followed by successive loss of $R^•$. Generally, the base peaks corresponded to $M_2(O_2CR')_4^+$.

The compounds $W_2R_2(O_2CR')_4$ undergo photoinduced elimination of $R^•$. The previously unknown compound $W_2(O_2CH)_4$ can be prepared in essentially quantitative yield by using a Hanovia low-pressure Hg lamp (eq 6). The presence of 1,4-cyclohexadiene in eq 6 acts as a hydrogen-atom donor and suppresses side reactions involving $R^•$.

$$W_2(np)_2(O_2CH)_4 + C_6H_8 \xrightarrow[\text{benzene}]{h\nu, 25 °C} W_2(O_2CH)_4 + C_6H_6 + 2Me_4C \quad (6)$$
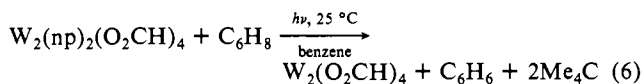
NMR Studies. The general feature in the NMR spectra of the $M_2R_2(O_2CR')_4$ compounds is the appearance of one type of carboxylate group and one type of alkyl ligand independent of temperature. This precludes an alternative structure of type II, which is found for $W_2R_2(O_2CNR'_2)_4$ compounds, assuming, of course, that interconversion of I and II is not rapid on the NMR time scale. As we show below this distinction can be made.


II
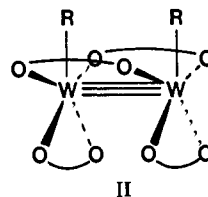
(35) Formic anhydride is unstable above −10 °C. Muramatsv, I.; Itoi, M.; Tsuji, A.; Hagitani, A. *Bull. Chem. Soc. Jpn.* **1964**, *37*, 756.
(36) Appleton, T. G.; Clark, H. C.; Manzer, L. M. *Coord. Chem. Rev.* **1973**, *10*, 335.
(37) Mowat, W.; Shortland, A.; Yagupski, G.; Hill, N. J.; Yagupski, M.; Wilkinson, G. *J. Chem. Soc., Dalton Trans.* **1972**, 533.

(38) When a pure sample of $W_2(np)_2(O_2CMe)_4$ was dissolved in toluene followed by introduction of $HNMe_2$, a brown oil was produced in a fashion akin to that observed in the reaction between $W_2(np)_2(NMe_2)_4$ and CH_3C-O_2H.

Tungsten-Tungsten Triple Bond. 13

J. Am. Chem. Soc., Vol. 109, No. 22, 1987 6799
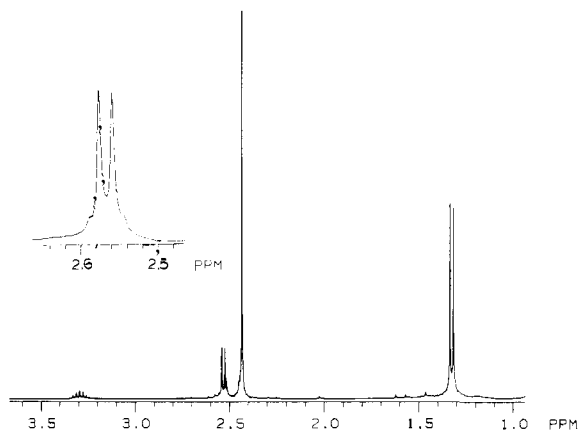
Figure 1. ^{1}H NMR spectrum of $W_2(i\text{-Bu})_2(O_2CMe)_4$ in benzene-d_6 at 360 MHz, 22 °C. Inset shows the methylene protons of the W-i-Bu moiety with coupling to both the neighboring methine proton and ^{183}W nuclei, $I = {}^1/_2$, 14.5% natural abundance.

The ^{1}H NMR spectrum of $W_2(i\text{-Bu})_2(O_2CMe)_4$ is shown in Figure 1 and is illustrative of the simplicity of these spectra. However, not all $W_2R_2(O_2CR')_4$ compounds conform to this simple behavior. There is evidence that certain compounds exist in two isomeric forms in solution, having structures I and II. The ^{1}H NMR spectra for $W_2Bz_2(O_2CEt)_4$ in toluene-d_8 and methylene-d_2 chloride are shown in Figure 2. Here a large single crystal of the compound was dissolved initially in CD_2Cl_2, and the ^{1}H NMR spectrum was recorded. The solution was evaporated to dryness, the resultant solid was redissolved in toluene-d_8, and the ^{1}H NMR spectrum was again recorded. At 22 °C, the equilibrium concentration of I to II is ca. 8:1 in toluene-d_8 and ca. 2:1 in CD_2Cl_2. Probably the more polar solvent favors the isomer with a dipole moment in the same way as is observed for *cis*- and *trans*-$PtCl_2(PR_3)_2$ compounds.[39] The attainment of equilibria between I and II is rapid but interconversions between I and II are not sufficiently rapid to be monitored by NMR coalescence at elevated temperatures. Studies of the dynamics and energetics for the interconversion of I and II are currently under way, and these results will be presented elsewhere.[40]

Table I summarizes our observations of structural types I and II in benzene-d_6 solutions. No bis(neopentyl) complex adopts structure II in solution: even the formate $W_2(np)_2(O_2CH)_4$ is exclusively in the form I, and its ^{1}H NMR spectrum is shown in Figure 3. However, for less bulky alkyl/aryl/benzyl ligands and with propionate, acetate, and formate as the carboxylate groups, the isomeric form II becomes favored. For $W_2Me_2(O_2CMe)_4$, the structural type II is found exclusively in solution. Regrettably, crystals suitable for a single-crystal X-ray study have not been obtained and so we have not been able to determine its isomeric form in the solid state.

One might be tempted to conclude from the data shown in Table I that the preference for structural type I or II is determined solely by the steric factors of the ligands, R and O_2CR', with a weighting factor R > R'. However, there are subtle electronic factors also at work. The presence of two syn-neopentyl ligands (structure type II) is found in $W_2R_2(O_2CNR'_2)_4$ (R = Me, np) compounds and in $W_2(np)_2(S_2CNEt_2)_2(O_2CMe)_2$, the latter compound being prepared in the reaction between $W_2(np)_2(O_2CMe)_4$ and NaS_2CNEt_2 (2 equiv) in the presence of acetic acid.[40]

Finally of note is the presence of coupling to ^{183}W, $I = {}^1/_2$, 14.5% natural abundance, $^2J_{^{183}W-H} \sim 8\text{-}17$ Hz for the hydrogen atoms on the α-carbon of the alkyl ligand R. *This coupling is only seen when the alkyl ligands are in the axial positions.* Compounds that exist in an equilibrium mixture of I and II do not show this coupling to α-hydrogen atoms of the alkyl ligands

Table II. Fractional Coordinates and Isotropic Thermal Parameters for the $W_2Bz_2(O_2CEt)_4$ Molecule

atom	10^4x	10^4y	10^4z	$10B_{iso}$, Å^2
W(1)	5309.7 (3)	475.0 (4)	5651.7 (2)	13
C(2)	5945 (12)	1472 (15)	6940 (7)	18
C(3)	6999 (9)	615 (10)	7378 (6)	16
C(4)	6852 (10)	-510 (11)	8043 (7)	21
C(5)	7855 (11)	-1328 (13)	8431 (7)	27
C(6)	9021 (10)	-1009 (14)	8200 (7)	25
C(7)	9186 (10)	107 (14)	7554 (7)	23
C(8)	8185 (9)	913 (13)	7155 (7)	18
O(9)	3659 (6)	-236 (7)	6141 (4)	16
C(10)	2841 (9)	-927 (11)	5631 (6)	19
O(11)	6965 (5)	1221 (7)	5185 (4)	15
C(12)	1640 (10)	-1333 (16)	5964 (7)	25
C(13)	714 (11)	-2109 (16)	5314 (8)	32
O(14)	6121 (5)	-1695 (7)	6011 (4)	15
C(15)	6065 (8)	-2841 (11)	5460 (6)	16
O(16)	4508 (5)	2667 (7)	5310 (4)	17
C(17)	6665 (13)	-4383 (14)	5698 (8)	23
C(18)	7483 (12)	-4364 (14)	6548 (9)	28

Table III. Fractional Coordinates and Isotropic Thermal Parameters for the $W_2(np)_2(O_2CEt)_4$ Molecule

atom	10^4x	10^4y	10^4z	$10B_{iso}$, Å^2
W(1)	1046.8 (1)	476.8 (1)	1265.1 (1)	8
O(2)	9338 (2)	1288 (2)	2027 (2)	11
O(3)	7211 (2)	313 (2)	-547 (2)	11
C(4)	2235 (2)	8937 (2)	9042 (2)	11
C(5)	6526 (3)	1715 (2)	1430 (3)	14
C(6)	7292 (3)	2516 (2)	3276 (3)	16
O(7)	945 (2)	8679 (2)	2330 (2)	12
O(8)	1186 (2)	2287 (2)	258 (2)	12
C(9)	-147 (2)	7653 (2)	1340 (3)	12
C(10)	9821 (3)	6333 (2)	2068 (3)	17
C(11)	8325 (4)	5261 (3)	866 (4)	24
C(12)	3287 (3)	1377 (2)	3669 (3)	15
C(13)	3274 (2)	2300 (2)	5217 (2)	12
C(14)	4873 (3)	7219 (3)	3435 (3)	18
C(15)	7609 (3)	6403 (2)	5349 (3)	18
C(16)	7552 (3)	8524 (3)	3924 (3)	19

Table IV. Fractional Coordinates and Isotropic Thermal Parameters for the $W_2(np)_2(O_2CH)_4$ Molecule

atom	10^4x	10^4y	10^4z	$10B_{iso}$, Å^2
W(1)	5363 (1)	3238 (1)	2355 (1)	51
O(2)	6342 (12)	2770 (12)	3028 (8)	56
C(3)	6273 (17)	1880 (23)	3211 (13)	63
O(4)	5620 (13)	1265 (11)	3016 (8)	56
O(5)	3653 (12)	2223 (12)	1701 (9)	63
C(6)	3738 (21)	3145 (23)	1500 (16)	74
O(7)	4421 (15)	3721 (12)	1721 (9)	73
C(8)	6246 (23)	4620 (21)	2478 (19)	94
C(9)	6200 (22)	5514 (18)	2058 (14)	63
C(10)	6324 (35)	5285 (24)	1437 (17)	113
C(11)	6888 (40)	6318 (31)	2240 (24)	167
C(12)	5178 (36)	5997 (27)	2068 (20)	115

in the isomeric form II. Also of note is the appearance of $^3J_{^{183}W-H}$ = 8 Hz to the formate hydrogen atoms. As shown in Figure 3, the tungsten satellites of the formate hydrogen are indicative of the $W_2(\mu\text{-}O_2CH)_4$ moiety, being of ca. 24% integral intensity.

In the ^{13}C NMR spectra of $W_2(np)_2(O_2CR')_4$ compounds the appearance of $^1J_{^{183}W-^{13}C} \sim 140$ Hz and $^2J_{^{183}W-^{13}C} \sim 14$ Hz is also worthy of note.

We believe that the coupling to ^{183}W reflects the significant W 6s orbital contribution to both the M–C and M–O σ bonds.[44]

Solid-State and Molecular Structures. Six compounds have been subjected to single-crystal X-ray studies, five $W_2R_2(O_2CR')_4$ compounds and $Mo_2(np)_2(O_2CMe)_4$. With the exception of $W_2(np)_2(O_2CH)_4$, good data sets were collected and refinement produced good-quality structural information. Regrettably, crystals of the formate underwent a gradual phase change on cooling and some fracturing of the crystal appeared to have oc-

(39) Basolo, F.; Pearson, R. G. *Mechanisms of Inorganic Reactions*; Wiley: New York, 1967; Chapter 5.

(40) Chisholm, M. H.; Clark, D. L.; Huffman, J. C.; Van Der Sluys, W. G. *J. Am. Chem. Soc.*, following paper in this issue.

Table V. Fractional Coordinates and Isotropic Thermal Parameters for the $W_2(np)_2(O_2CPh)_4$ Molecule

atom	10^4x	10^4y	10^4z	$10B_{iso}$, $Å^2$
W(1)	5216.6 (3)	381.2 (3)	5636.3 (2)	9
O(2)	6152 (5)	−1280 (5)	6165 (3)	13
C(3)	6196 (7)	−2186 (7)	5681 (5)	14
O(4)	5669 (5)	−2070 (5)	4875 (3)	12
C(5)	6824 (7)	−3370 (7)	6057 (5)	14
C(6)	6624 (8)	−4446 (7)	5560 (5)	18
C(7)	7202 (9)	−5557 (8)	5930 (6)	23
C(8)	8011 (10)	−5609 (8)	6783 (5)	24
C(9)	8246 (9)	−4534 (8)	7271 (5)	24
C(10)	7651 (9)	−3419 (8)	6917 (5)	20
O(11)	3376 (5)	−308 (5)	5613 (3)	12
C(12)	2601 (7)	−892 (6)	4956 (4)	11
O(13)	2936 (5)	−1081 (5)	4318 (3)	12
C(14)	1310 (7)	−1389 (7)	4934 (5)	16
C(15)	460 (8)	−2021 (8)	4230 (5)	19
C(16)	−747 (8)	−2501 (8)	4223 (5)	22
C(17)	−1120 (8)	−2350 (8)	4906 (6)	21
C(18)	−283 (9)	−1721 (8)	5608 (6)	21
C(19)	926 (7)	−1223 (8)	5625 (5)	16
C(20)	5529 (7)	1261 (7)	6839 (4)	13
C(21)	6397 (7)	728 (7)	7707 (4)	14
C(22)	5795 (10)	−507 (8)	7882 (5)	21
C(23)	6379 (9)	1690 (9)	8375 (5)	21
C(24)	7861 (8)	535 (8)	7792 (5)	19

Table VI. Fractional Coordinates and Isotropic Thermal Parameters for the $W_2(np)_2(O_2CMe)_2(O_2CCF_3)_2$ Molecule

atom	10^4x	10^4y	10^4z	$10B_{iso}$, $Å^2$
W(1)	3786 (1)	2344 (1)	3749 (1)	27
W(2)	2279 (1)	1818 (1)	3765 (1)	22
O(3)	4212 (9)	1457 (10)	4982 (11)	29
C(4)	3559 (15)	968 (13)	5335 (16)	26
O(5)	2702 (9)	925 (10)	5007 (11)	30
C(6)	3868 (15)	331 (4)	6222 (18)	28
F(7)	4903 (16)	177 (17)	6247 (19)	113
F(8)	3719 (17)	667 (15)	7221 (17)	101
F(9)	3480 (19)	−362 (16)	6184 (19)	117
O(10)	4166 (9)	1454 (9)	2493 (11)	28
C(11)	3540 (15)	952 (15)	2131 (17)	32
O(12)	2673 (9)	934 (9)	2500 (11)	28
C(13)	3823 (19)	352 (19)	1229 (19)	44
F(14)	4678 (17)	42 (19)	1334 (20)	140
F(15)	3208 (21)	−294 (15)	1117 (21)	126
F(16)	3790 (16)	685 (12)	266 (15)	84
O(17)	3375 (10)	3232 (9)	2557 (13)	36
C(18)	2452 (14)	3253 (15)	2162 (17)	32
O(19)	1849 (10)	2696 (9)	2541 (11)	29
C(20)	2172 (15)	3834 (15)	1298 (19)	36
O(21)	3401 (9)	3176 (10)	4924 (14)	47
C(22)	2547 (15)	3217 (12)	5435 (21)	34
O(23)	1868 (10)	2661 (9)	4996 (11)	31
C(24)	2227 (15)	3798 (15)	6282 (18)	35
C(25)	5332 (17)	2705 (17)	3507 (27)	55
C(26)	5796 (14)	3501 (14)	3984 (17)	31
C(27)	5225 (16)	4335 (14)	3644 (18)	37
C(28)	5829 (15)	3463 (16)	5251 (21)	44
C(29)	6889 (23)	3497 (28)	3605 (28)	95
C(30)	872 (14)	1165 (15)	3579 (18)	33
C(31)	−94 (15)	1642 (15)	3993 (17)	32
C(32)	−100 (20)	1558 (27)	5307 (26)	81
C(33)	−262 (15)	2499 (23)	3597 (32)	77
C(34)	−936 (18)	923 (26)	3666 (23)	72

Table VII. Fractional Coordinates and Isotropic Thermal Parameters for the $Mo_2(np)_2(O_2CMe)_4$ Molecule

atom	10^4x	10^4y	10^4z	$10B_{iso}$, $Å^2$
Mo(1)	−610.6 (1)	282.8 (2)	−1133.4 (2)	10
O(2)	8533 (1)	2967 (2)	304 (1)	13
C(3)	−1095 (2)	3443 (2)	1916 (2)	13
O(4)	−189 (1)	2364 (2)	2667 (1)	13
C(5)	−1766 (2)	5295 (2)	2952 (2)	16
O(6)	1228 (1)	1405 (2)	−1161 (1)	13
C(7)	2420 (2)	1420 (2)	29 (1)	13
O(8)	2508 (1)	784 (2)	1202 (1)	13
C(9)	3751 (2)	2200 (3)	35 (2)	17
C(10)	−1796 (2)	585 (2)	−3602 (2)	14
C(11)	−2809 (2)	2345 (2)	−3828 (2)	12
C(12)	−1918 (2)	4043 (2)	−3087 (2)	16
C(13)	6575 (2)	1962 (3)	4251 (2)	18
C(14)	−4153 (2)	2765 (3)	−3040 (2)	16

for the related d^4–d^4 $M_2(O_2CR')_4$ compounds in Table IX. The following points are worthy of note.

1. The W–W distances are essentially identical in the d^3–d^3 and d^4–d^4 compounds.[22,33,41]

2. The Mo–Mo distances in $Mo_2(O_2CMe)_4$ and $Mo_2(np)_2$-$(O_2CMe)_4$ differ significantly, with the d^3–d^3 dinuclear compound having the longer distance.[13] However, for Mo_2^{6+}-containing compounds, the Mo–Mo distance, 2.1302 (6) Å, is the shortest known.

3. For related pairs of compounds the M–O distances are essentially identical.[13,22,33,41] In $W_2(np)_2(O_2CMe)_2(O_2CCF_3)_2$, the W–O bond distances to the CF_3COO^- ligands are notably longer than those to the acetate ligands, consistent wih the greater electron-releasing properties and greater trans influence of the latter.[36]

4. The M–C distances, which fall in the range 2.17–2.21 Å, are typical of those seen for alkyl/benzyl ligands bonded to $(M≡M)^{6+}$ centers.[42,43]

Bonding Considerations. It is appropriate to summarize briefly the results of a previous relativistic SCF–Xα–SW calculation on the model compounds $W_2(O_2CH)_4$ and $W_2(O_2CH)_4(CH_3)_2$.[44] The latter compound may be viewed as resulting from the interaction of two CH_3· radicals with the d^4–d^4 compound W_2-$(O_2CH)_4$. The correlation energy diagram shown in Figure 10 uses this approach.

1. Although the simple view of the M–M quadruple bond being formed from combining two d^4 fragments is often represented as $\sigma^2\pi^4\delta^2$, for the heavier element W in $W_2(O_2CH)_4$ the valence 6s orbital plays a significant role due to relativistic effects. There really are two significant components to the M–M σ bond arising from W–W 6s–6s and $5d_{z^2}$–$5d_{z^2}$ interactions. These lead to the $5a_{1g}$ and $4a_{1g}$ MOs, respectively.[45] Both of these MOs have M–O bonding components: the $5d_{z^2}$ component is M–O bonding through the doughnut but the 6s component is of opposite sign and thus M–O antibonding.

2. The interaction with the two CH_3· radicals along the W–W axis leaves the $\pi^4\delta^2$ W–W bonding manifold relatively unperturbed.

3. The heart of the bonding in $W_2(CH_3)_2(O_2CH)_4$, summarized by the diagram shown in Figure 10, reveals that the in-phase, a_g, and out-of-phase, b_u, combinations of the CH_3· orbitals interact with W–W σ-bonding ($4a_{1g}$ and $5a_{1g}$) and antibonding ($5a_{2u}$) orbitals of $W_2(O_2CH)_4$. The totally symmetric a_g interaction leads to a stabilization of two W–W σ-bonding orbitals ($10a_g$ and $13a_g$ in Figure 10) while the interaction with the W–W σ* orbital

curred even at −50 °C, the temperature at which data were finally collected.

Fractional coordinates are given in Tables II–VII and a summary of crystal data is given in Table VIII. ORTEP views of the molecules showing the atom numbering schemes used in the tables are given in Figures 4–9. For the sake of brevity, listings of bond distances and angles have been deposited with the remainder of the crystallographic data in the supplementary materials. We do, however, present a summary of pertinent bond distances and angles for the $M_2R_2(O_2CR')_4$ compounds together with parameters

(41) Cotton. F. A.; Wang, W. *Inorg. Chem* **1984**, *23*, 1604.

(42) Chisholm, M. H.; Eichhorn, B. W.; Huffman, J. C. *J. Chem. Soc., Chem. Commun.* **1985**, 861.

(43) Chetcuti, M. J.; Chisholm, M. H.; Folting, K.; Huffman, J. C.; Janos, J. *J. Am. Chem. Soc.* **1982**, *104*, 4684.

(44) Braydich, M. D.; Bursten, B. E.; Chisholm, M. H.; Clark, D. L. *J. Am. Chem. Soc.* **1985**, *107*, 4459.

(45) Xα–SW calculations on $M_2(O_2CH)_4$ systems (where M is a second- or third-row transition metal) in general yield two components of the metal–metal σ bond, the $4a_{1g}$ and $5a_{1g}$ MOs. However, in the case of Mo, valence 5s and $4d_{z^2}$ mixing is not nearly so pronounced, presumably due to the greater relativistic stabilization of W 6s than Mo 5s orbitals. See ref 17, 44, and 71e).

Table VIII. Summary of Crystal Data[a]

	I	II	III	IV	V	VI
empirical formula	$W_2C_{26}H_{34}O_8$	$W_2C_{22}H_{42}O_8$	$W_2C_{38}H_{42}O_8$	$W_2C_{14}H_{26}O_8$	$W_2C_{18}H_{28}F_6O_8$	$Mo_2C_{18}H_{34}O_8$
color of crystal	orange-red	black	dark red	black	dark red	orange
crystal dimens, mm	0.12 × 0.10 × 0.10	0.20 × 0.20 × 0.17	0.07 × 0.07 × 0.09	0.12 × 0.12 × 0.14	0.15 × 0.22 × 0.20	0.12 × 0.13 × 0.13
space group	$P2_1/c$	$P\bar{1}$	$P2_1/c$	$I4_1/a$	$P2_1/n$	$P\bar{1}$
cell dimens						
temp, °C	−157	−164	−157	−50	−158	−157
a, Å	10.877 (5)	9.000 (2)	10.693 (4)	13.295 (9)	13.515 (4)	9.400 (2)
b, Å	8.414 (3)	9.752 (2)	10.714 (4)	13.295 (9)	15.452 (5)	7.745 (2)
c, Å	15.153 (7)	8.699 (2)	17.077 (8)	22.476 (13)	12.010 (3)	8.782 (2)
α, deg		96.53 (1)				112.54 (1)
β, deg	94.65 (3)	117.35 (1)	111.98		90.09 (2)	107.64 (1)
γ, deg		92.97 (1)				77.47 (1)
Z (molecules/cell)	2	1	2	8	4	1
volume, Å³	1382.18	669.05	1814.39	3972.79	2508.11	559.03
calcd density, g/cm³	2.024	1.991	1.869	2.307	2.262	1.694
wavelength, Å	0.71069	0.71069	0.71069	0.71069	0.71069	0.71069
mol wt	842.25	802.27	994.45	690.05	854.10	570.34
linear absorp coeff, cm⁻¹	85.391	88.15	66.930	118.565	94.451	11.328
detector-to-sample dist, cm	22.5	22.5	22.5	22.5	22.5	22.5
sample-to-source dist, cm	23.5	23.5	23.5	23.5	23.5	23.5
av ω scan width at half-height	0.25	0.25	0.25	0.25	0.25	0.25
scan speed, deg/min	4.0	4.0	4.0	4.0	4.0	4.0
scan width, deg + disp	2.0	2.0	2.0	2.0	2.0	2.0
indiv bkgd, s	8	8	4	8	8	6
aperture size, mm	3.0 × 4.0	3.0 × 4.0	3.0 × 4.0	3.0 × 4.0	3.0 × 4.0	3.0 × 4.0
2θ range, deg	6–45	6–75	6–55	6–45	6–45	6–45
total no. of reflections collected	2118	15673	4745	2605	3684	5614
no. of unique intensities	1814	7070	4190	1315	3288	4932
no. of $F > 3.00\sigma(F)$	170		3403	1030	2924	
no. of $F > 3.0\sigma(F)$		6942				4785
$R(F)$	0.0349	0.0214	0.0404	0.0641	0.0659	0.0288
$R_w(F)$	0.0362	0.0202	0.0401	0.0589	0.0659	0.0322
goodness of fit for last cycle	1.440	1.384	0.921	1.459	1.982	0.844
max Δ/σ for last cycle	0.05	0.05	0.05	0.05	0.05	0.05

[a] I = $W_2Bz_2(O_2CEt)_4$, II = $W_2(np)_2(O_2CEt)_4$, III = $W_2(np)_2(O_2CPh)_4$, IV = $W_2(np)_2(O_2CH)_4$, V = $W_2(np)_2(O_2CMe)_2(O_2CCF_3)_2$, and VI = $Mo_2(np)_2(O_2CMe)_4$.

Table IX. Selected Bond Distances (Å) and Angles (Deg) for $M_2R_2(O_2CR')_4$ Molecules and $M_2(O_2CR')_4$ Molecules (M = Mo, W)

compd[a]	M–M	M–C	W–O(ax)	M–O[b]	M–M–C[b]	M–M–O[b]
$W_2Bz_2(O_2CEt)_4$	2.1859 (12)	2.184 (10)		2.084 (6)	178.7 (4)	90.52 (17)
$W_2(np)_2(O_2CEt)_4$	2.1911 (7)	2.1752 (21)		2.087 (1)	174.4 (1)	90.57 (5)
$W_2(np)_2(O_2CH)_4$	2.1870 (23)	2.20 (3)		2.060 (19)	170.3 (9)	90.6 (4)
$W_2(np)_2(O_2CPh)_4$	2.2026 (11)	2.170 (7)		2.082 (5)	175.15 (11)	90.46 (7)
$W_2(np)_2(O_2CMe)_2(O_2CCF_3)_2$	2.1935 (13)	2.183 (24)		2.043 (15)	170.2 (8)	90.4 (4)
		2.164 (20)		2.106 (14)	171.1 (6)	89.9 (4)
$Mo_2(np)_2(O_2CMe)_4$	2.1302 (6)	2.1923 (17)		2.1029 (13)	174.50 (4)	91.34 (4)
$W_2(O_2CEt)_4$[c]	2.189 (1)		2.655 (4)	2.085 (4)		
$W_2(O_2CPh)_4(THF)_2$[d]	2.196 (1)		2.628 (8)	2.077 (4)		
$Mo_2(O_2CMe)_4$[e]	2.0934					

[a] Due to the symmetry of $W_2(np)_2(O_2CMe)_2(O_2CCF_3)_2$, there are two W–C bond lengths and two separate W–O(av) bond lengths. The W–O bond lengths of the TFA ligands are 2.106 (14) Å. [b] Bond lengths and angles were averaged where appropriate. [c] Reference 23. [d] Reference 41. [e] Reference 13.

produces a new MO, $15b_u$, which has some W–W σ^* character but is mostly W–C bonding. The net result is that the W–W σ bonding in $W_2(CH_3)_2(O_2CH)_4$ is not destroyed but merely mixed with the W–C and W–O σ bonding. There are now three orbitals having significant W–W σ character, the $10a_g$, $13a_g$, and $15b_u$; the former two are W–W σ bonding and only the latter is W–W σ antibonding. All three W–W σ-type orbitals have some W–C

σ-bonding character; in particular, the $15b_u$ orbital is strongly W–C bonding and only weakly W–W antibonding.

This bonding picture correlates well with the observed structural data. In particular, the W–W distances in $W_2R_2(O_2CR')_4$ and $W_2(O_2CR')_4$[33,41] compounds are essentially identical, even though in a formal sense they are d^3–d^3 and d^4–d^4 compounds having M–M triple and quadruple bonds, respectively. Furthermore, the
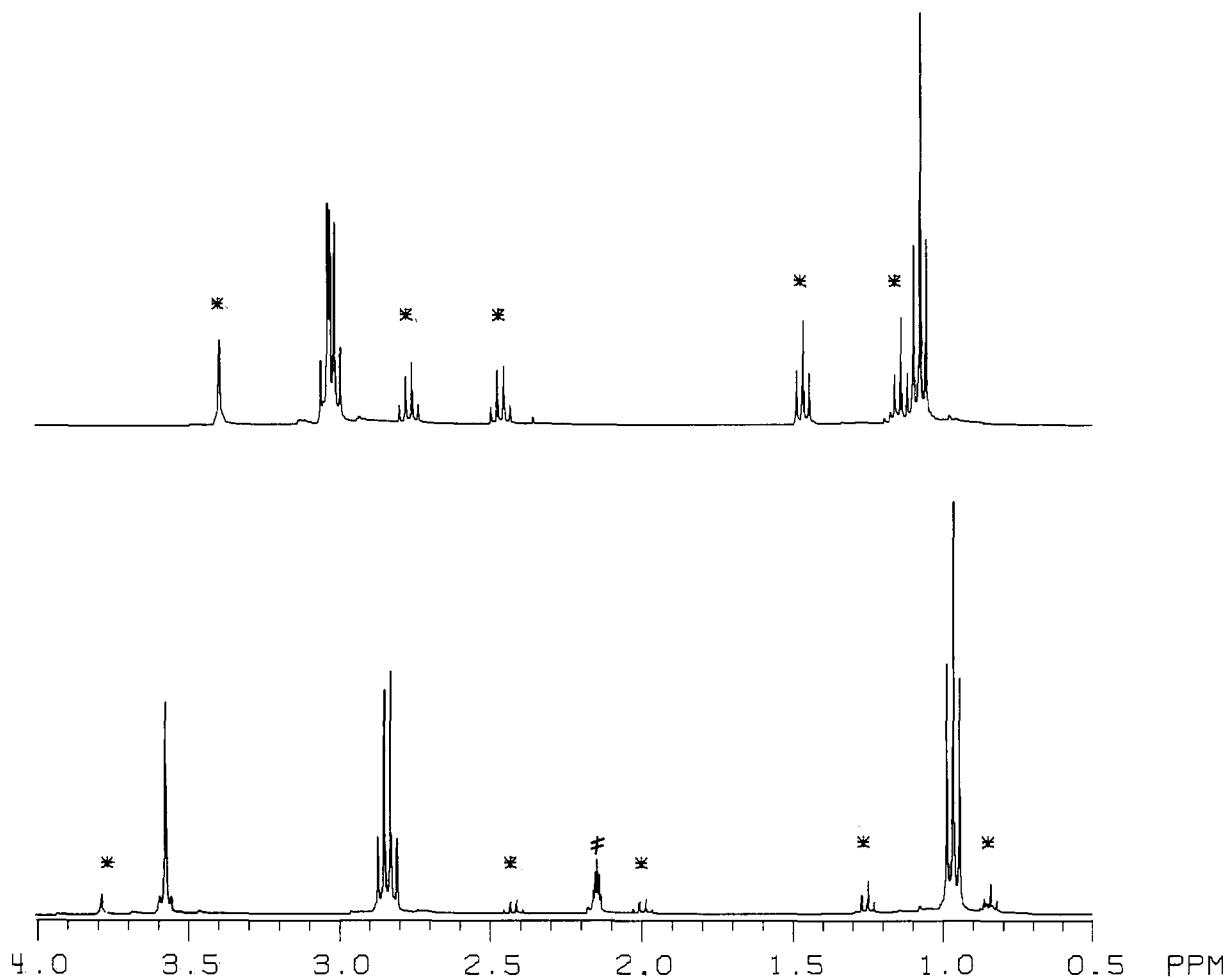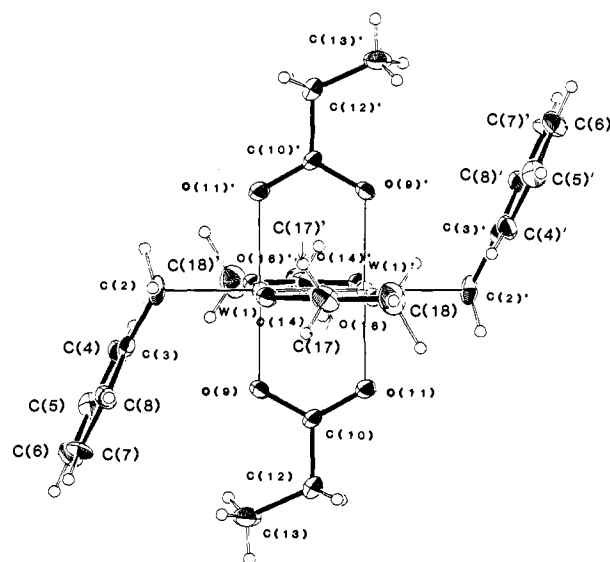
Figure 2. ^{1}H NMR spectra of $W_2Bz_2(O_2CEt)_4$ in toluene-d_8 (bottom spectrum) and CD_2Cl_2 (top spectrum) showing the presence of two isomers, I and II, defined in the text, and the solvent dependence on the equilibrium concentrations of each. The proton signals denoted by an asterisk correspond to isomer II, and the residual protons in toluene-d_8 in the lower spectrum are denoted by a dagger. The spectra were recorded at 360 MHz and 22 °C. The CH_2Ph protons of isomer I in CD_2Cl_2 are partially obscured by the $O_2CCH_2CH_3$ signals.
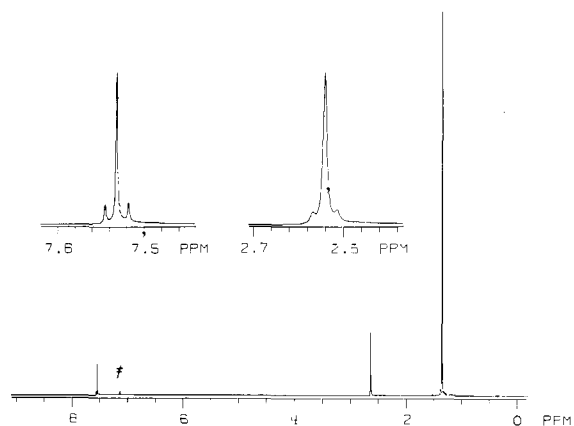
Figure 3. ^{1}H NMR spectrum (360 MHz, 22 °C, benzene-d_6) of W_2-$(np)_2(O_2CH)_4$. Insets at scale expansion show the formate proton signals, ca. δ 7.5, and the methylene protons of the np ligand, ca. δ 2.6. The protio impurity in the benzene-d_6 is denoted by a dagger.

Figure 4. ORTEP drawing of the $W_2Bz_2(O_2CEt)_4$ molecule showing the atom number scheme used in the tables.

M—O distances are the same for $M_2R_2(O_2CR')_4$ and $M_2(O_2CR')_4$ compounds.[13,22,33,41] This is consistent with the occupation of the M—M δ orbital in both. If the M—M δ orbital was not occupied in the $W_2R_2(O_2CR')_4$ compounds, we would expect shorter W—O distances relative to those seen in $W_2(O_2CR')_4$ compounds. This point has previously been discussed in the context of the compounds of formula $Mo_2(OR)_6L_2$ and $Mo_2(OR)_4L_4$.[46]

If we now turn to the structural parameters of the Mo_2-

$(np)_2(O_2CMe)_4$ and $Mo_2(O_2CMe)_4$[13] compounds, we note a small ca. 0.04-Å increase in Mo—Mo distance for the d^3–d^3 dimer relative to the d^4–d^4 dimer. The Mo—O distances are essentially identical. Though a calculation has not been performed on $Mo_2(CH_3)_2$-$(O_2CH)_4$, a comparison of the bonding in $M_2(O_2CH)_4$ compounds
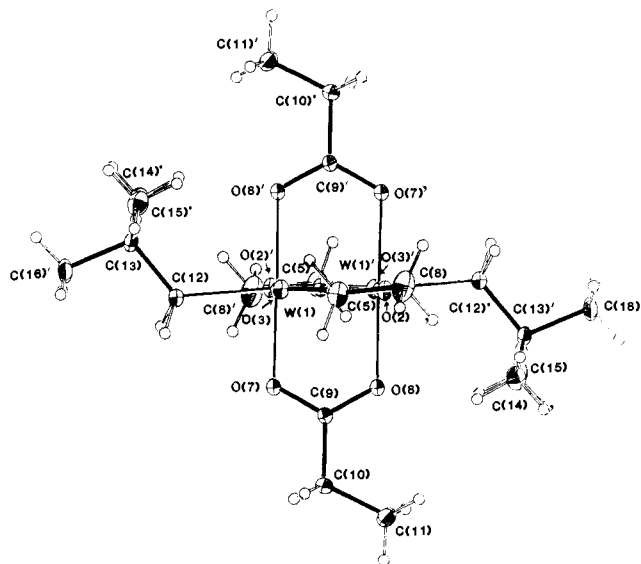
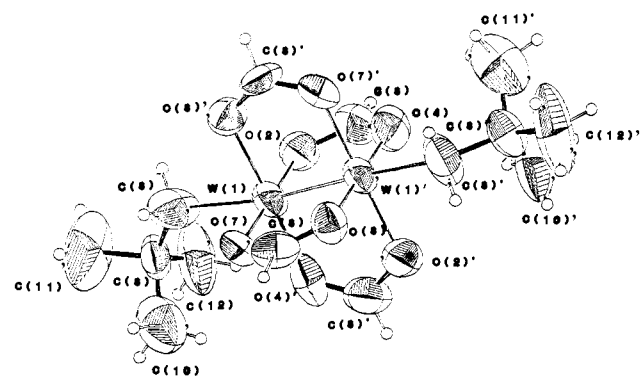**Figure 5.** ORTEP drawing of the $W_2(np)_2(O_2CEt)_4$ molecule showing the atom number scheme used in the tables.

Figure 6. ORTEP view of the $W_2(np)_2(O_2CH)_4$ molecule showing the atom number scheme used in the tables.

Figure 7. ORTEP view of the $W_2(np)_2(O_2CPh)_4$ molecule showing the atom number scheme used in the tables.

Figure 8. ORTEP view of the $W_2(np)_2(O_2CMe)_2(O_2CCF_3)_2$ molecule showing the atom number scheme used in the tables.

Figure 9. ORTEP view of the $Mo_2(np)_2(O_2CMe)_4$ molecule showing the atom number scheme used in the tables.

(Mo = Mo and W) has been undertaken. The relativistic effects are more important for tungsten than molybdenum and the M–M σ bond in $Mo_2(O_2CR')_4$ compounds has proportionally greater metal d_{z^2} character.[45] In other words the simplistic description of the quadruple bond as $\sigma^2\pi^4\delta^2$ is more appropriate for Mo_2-$(O_2CR')_4$ compounds. On the basis of the orbital interaction diagram shown in Figure 10, we would anticipate that the introduction of two CH_3• radicals would have a greater perturbation on the Mo–Mo σ bonding. The Mo–C σ-bonding MO which represents the out-of-phase M–M σ (antibonding) MO ($15b_u$ in Figure 10) would be proportionally higher in energy. Its position relative to the M–M δ-bonding MO is clearly uncertain in the absence of either a calculation or experimental data.

Thus, before we proceed to present the experimental data pertaining to UV–visible spectroscopy, photoelectron spectroscopy, and electrochemistry, we note that we anticipate that the M–M $\pi^4\delta^2$ configuration is preserved in the $M_2R_2(O_2CR')_4$ compounds. The location of the M–C σ-bonding and M–M σ-antibonding MO ($15b_u$) relative to the M–M π and δ orbitals remains a matter for further consideration.

Electrochemistry. From the calculations presented elsewhere[44] and the discussion above we should expect that both $M_2(O_2CR')_4$ and $M_2R_2(O_2CR')_4$ (M = Mo, W) complexes would exhibit similar electrochemical properties, and the nature of the supporting carboxylate ligands should also influence the potential at which these compounds undergo redox reactions in a common manner.
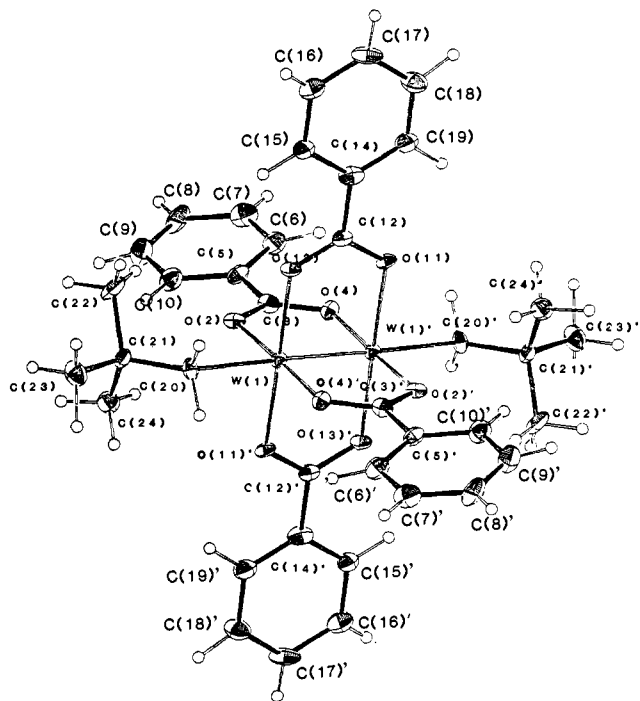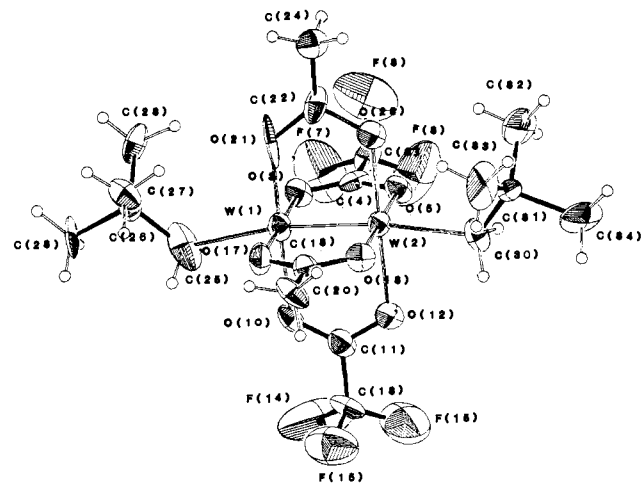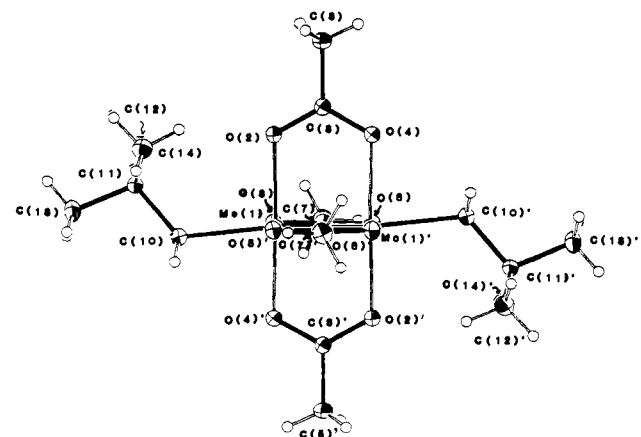
(46) (a) Chisholm, M. H. *Polyhedron* **1983**, *2*, 681. (b) Chisholm, M. H.; Folting, K.; Huffman, J. C.; Tatz, R. J. *J. Am. Chem. Soc.* **1984**, *106*, 1153.

Table X. Electrochemical Data for $M_2(O_2CR')_4$ (M = Mo, W) and $W_2R_2(O_2CR')_4$ Type Molecules[a]
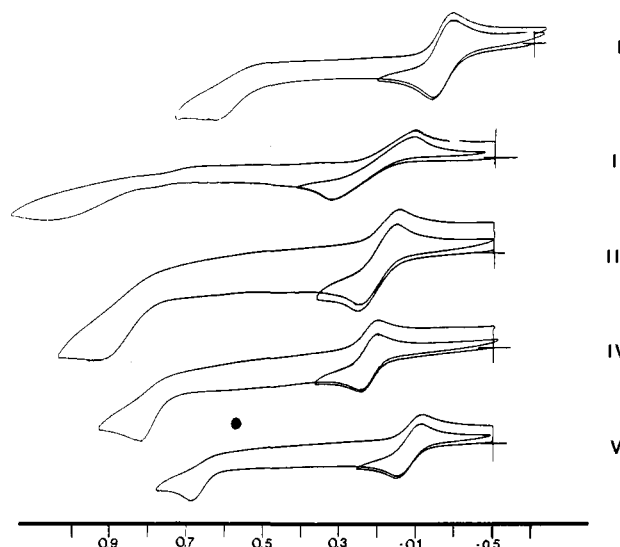
compd	solvent	1st ox $E_{1/2}$, V	ΔE_p, mV	i_{pc}/i_{pa}	% e[b]	2nd ox E_p, V
$Mo_2(O_2CEt)_4$	CH_2Cl_2	0.30	140	0.92		1.54
$W_2(O_2CEt)_4$	CH_2Cl_2	−0.28	93	1.11	98.0	0.79
$W_2(O_2CPh)_4$	CH_2Cl_2	−0.25	80	0.98		1.08
$Mo_2(np)_2(O_2CMe)_4$	CH_2Cl_2	0.58	185	0.89		2.09
$W_2(np)_2(O_2CMe)_4$	CH_2Cl_2	0.05	225	1.13		1.55
	CH_3CN	0.03	90	0.95		1.20
$W_2(np)_2(O_2CEt)_4$	CH_2Cl_2	0.04	170	1.08	103.3	1.32
	CH_3CN	−0.03	85	1.01		1.29
$W_2(np)_2(O_2CPh)_4$	CH_2Cl_2	0.07	80	1.03		1.14
$W_2(np)_2(O_2CPhOMe)_4$	CH_2Cl_2	−0.12	80	0.91		0.87
$W_2(np)_2(O_2CCF_3)_4$	CH_2Cl_2	1.51				
Cp_2Fe	CH_2Cl_2	0.14	77			
	CH_3CN	−0.08	70			

[a] Cyclic voltammograms were run at 200 mV/s and reference against a Ag/Ag$^+$ electrode. [b] The percentage of an electron removed by coulometry with the potential set at 0.1 V positive of $E_{1/2}$.
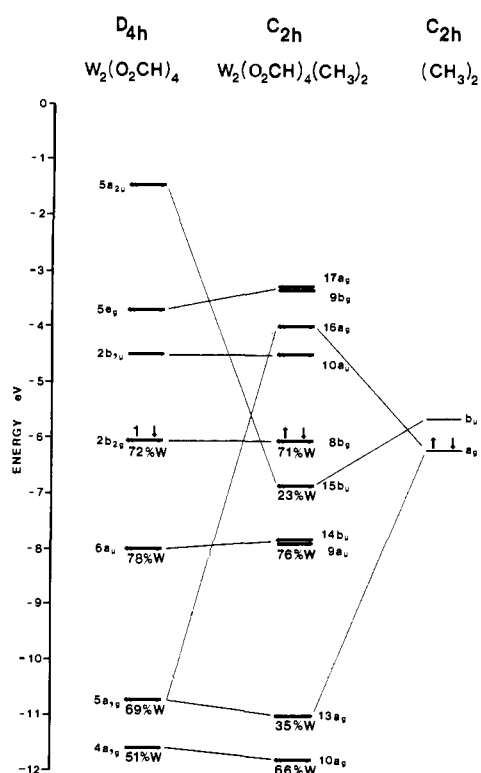
Figure 10. Results of the relativistic SCF-Xα-SW calculations on $W_2(O_2CH)_4(CH_3)_2$. This diagram shows the correlation of the orbitals of $W_2(O_2CH)_4(CH_3)_2$ to those of $W_2(O_2CH)_4$ and $(CH_3)_2$. Only those levels involved in W-W bonding or antibonding are shown. The HOMOs are denoted by use of spin-paired arrows (taken from ref 44).

Figure 11. Cyclic voltammograms recorded in CH_2Cl_2 referenced against a Ag/Ag$^+$ electrode at 200 mV/s for $W_2(O_2CEt)_4$ (I), $W_2(np)_2$-$(O_2CMe)_4$ (II), $W_2(np)_2(O_2CEt)_4$ (III), $W_2(np)_2(O_2CPh)_4$ (IV), and $W_2(np)_2(O_2CC_6H_4$-p-OMe)$_4$ (V).

Both of these classes of compounds are electrochemically active and were studied by cyclic voltammetry in CH_2Cl_2 and CH_3CN solutions. The electrochemical oxidations of $W_2(O_2CR')_4$ and $W_2R_2(O_2CR')_4$ molecules proceed in two discrete steps. No reduction couples were observed up to the solvent limit of −2.0 V. Representative cyclic voltammograms are shown in Figure 11, and a summary of the electrochemical data is given in Table X. In general, the first couple exhibits some reversible behavior, but the second is chemically irreversible and exhibits no reverse coupled wave over the scan rates studied (20–500 mV/s). The effect of the carboxylate is dramatically demonstrated by the large shift to positive potential of the first oxidation of $W_2(np)_2$-$(O_2CCF_3)_4$ (1.51 V) as compared to $W_2(np)_2(O_2CMe)_4$ (0.05 V). Similar behavior has been observed by Bear et al. in studies of acetamido-bridged Rh(II) dimers, which show a great dependence of $E_{1/2}$ with R and R' substituents of the $[R'NC(O)R]^-$ bridges,[47-50] and the carboxylate-bridged Rh(II) dimers, which have R and axial ligand dependencies.[51]

The first oxidative couple of $W_2R_2(O_2CR')_4$ is not completely reversible under the conditions employed here. The ratio of cathodic to anodic peak currents (i_{pc}/i_{pa}) was close to unity for the first oxidations, indicating that no chemical reactions occur at rates competitive with scan rates. In addition, plots of i_p vs. (scan rates)$^{1/2}$ yielded straight lines, indicating a diffusion-controlled process. However, the peak separations (ΔE_p) between the anodic and cathodic waves were in the range 80–225 mV in CH_2Cl_2. Two compounds were examined in CH_3CN and the ΔE_p was found to be smaller in this solvent than in CH_2Cl_2 (see Table X). These values can be compared to those of ferrocene in these same solvents, which produced values of 77 (CH_2Cl_2) and 70 mV (CH_3CN).[52] This suggests that the couples are not completely

(47) Duncan, J.; Malinski, T.; Zhu, T. P.; Hu, Z. S.; Kadish, K. M.; Bear, J. L. *J. Am. Chem. Soc.* **1982**, *104*, 5507.

(48) Kadish, K. M.; Lancon, D.; Dennis, A. M.; Bear, J. L. *Inorg. Chem.* **1982**, *21*, 2987.

(49) Dennis, A. M.; Korp, J. D.; Bernal, I.; Howard, R. A.; Bear, J. L. *Inorg. Chem.* **1983**, *22*, 1522.

(50) (a) Zhu, T. P.; Ahsan, M. Q.; Malinski, T.; Kadish, K. M.; Bear, J. L. *Inorg. Chem.* **1984**, *23*, 2. (b) Bear, J. L.; Zhu, T. P.; Malinski, T.; Dennis, A. M.; Kadish, K. M. *Inorg. Chem.* **1984**, *23*, 674.

(51) Das, K.; Kadish, K. M.; Bear, J. L. *Inorg. Chem.* **1978**, *17*, 930.

(52) Many other workers have found that under similar experimental conditions, ferrocene does not exhibit the expected ΔE_p = 59 mV; see, for example: (a) Gagne, R. *Inorg. Chem.* **1980**, *19*, 2854. (b) Brisdon, B. J.; Conner, K. A.; Walton, R. A. *Organometallics* **1983**, *2*, 1159. (c) Reference 22.

Tungsten–Tungsten Triple Bond. 13

J. Am. Chem. Soc., Vol. 109, No. 22, 1987 6805

Table XI. Low-Energy PES Ionization Potentials, FWHM, and Assignments for a Series of $M_2R_2(O_2CR')_4$ and $M_2(O_2CR')_4$ Compounds[a]

compd	IP, eV	fwhm, eV	orbital	positive ion state
I	6.17	0.26	δ	^2B_g
	7.69	0.85	$\pi + \sigma_{(wc)}$	$(^2B_u, {}^2A_u) + {}^2B_u$
	9.50		$\sigma_{(wc)}$	^2A_g
II	6.25	0.27	δ	^2B_g
	7.74	0.90	$\pi + \sigma_{(wc)}$	$(^2B_u, {}^2A_u) + {}^2B_u$
	9.75		$\sigma_{(wc)}$	^2A_g
III	6.77	0.24	δ	^2B_g
	8.12	0.86	$\pi + \sigma_{(wc)}$	$(^2B_u, {}^2A_u) + {}^2B_u$
	9.90		$\sigma_{(wc)}$	^2A_g
IV	7.68	0.29	δ	^2B_g
	8.65	0.79	$\sigma_{(wc)}$	^2B_u
	8.94	0.65	π	$(^2B_u, {}^2A_u)$
	10.50		$\sigma_{(wc)}$	^2A_g
V	6.90	0.30	δ	^2B_g
	7.42	0.60	$\sigma_{(Mo-C)}$	^2B_u
	8.41	0.54	π	$(^2B_u, {}^2A_u)$
	9.40		$\sigma_{(Mo-C)}$	^2A_g
VI	5.77	0.27	δ	$^2B_{2g}$
	7.68	0.66	π	^2E_u
	8.40	0.21	σ	$^2A_{1g}$
VII	6.07	0.26	δ	$^2B_{2g}$
	7.84	0.65	π	^2E_u
	8.54	0.22	σ	$^2A_{1g}$
VIII	6.19	0.27	δ	$^2B_{2g}$
	7.95	0.66	π	^2E_u
	8.62	0.21	σ	$^2A_{1g}$
IX	7.39		δ	$^2B_{2g}$
	9.01		π	^2E_u
	9.71		σ	$^2A_{1g}$
X	7.0		δ	$^2B_{2g}$
	8.8		$\pi + \sigma$	$^2E_u + {}^2A_{1g}$

[a] I = $W_2(np)_2(O_2CEt)_4$, II = $W_2(np)_2(O_2CMe)_4$, III = $W_2(np)_2$-$(O_2CH)_4$, IV = $W_2(np)_2(O_2CCF_3)_4$, V = $Mo_2(np)_2(O_2CMe)_4$, VI = $W_2(O_2C-t-Bu)_4$, VII = $W_2(O_2CMe)_4$, VIII = $W_2(O_2CCD_3)_4$, IX = $W_2(O_2CCF_3)_4$,[25] and X = $Mo_2(O_2CMe)_4$.[23]

Figure 12. He(I) photoelectron spectra in the low-energy region, 6.0–11.0 eV, for $W_2(np)_2(O_2CR')_4$ where R' = Me (a), H (b), and CF_3 (c).

reversible with respect to electron transfer.[53,54] One interesting observation is that the electron-transfer process of the W_2-$(np)_2(O_2CR')_4$ compounds, where R = C_6H_5 and p-C_6H_4OMe, is apparently more facile than for their aliphatic counterparts as indicated by their smaller ΔE_p's. A reasonable explanation of this may lie in the fact that if the axial sites of these compounds are occupied by alkyl groups, the distance an electron would necessarily have to traverse in the outer-sphere electron-transfer process would be further than for $M_2(O_2CR)_4$ complexes. If the carboxylate has a functional group such as an aryl ring, which may be conjugated through the carboxylate π system with the δ orbital, this would facilitate the removal of an electron from the δ orbital. Further arguments with respect to this conjugation effect will be made in the context of the electronic absorption spectra of these molecules (vide infra).

Oxidative coulometry at a potential 0.1 V more positive than $E_{1/2}$ for two representative molecules [$W_2(np)_2(O_2CEt)_4$ and $W_2(O_2CEt)_4$] showed that the first oxidative wave corresponds to the removal of one electron. Upon completion of the electrolysis, the solution had changed from green to dark brown, and a cyclic voltammogram showed no electrochemically active species was present in solution. Also, when the potential was set at 0.1 V more negative than the $E_{1/2}$, no current was passed when reductive coulometry was attempted. The oxidized species is apparently not stable for indefinite periods of time under our experimental conditions.

The qualitative similarities in electrochemistry between the d^3–d^3 and d^4–d^4 dimers is striking (Figure 11). The $E_{1/2}$ for the initial oxidation of $W_2(O_2CEt)_4$ is at a slightly more negative
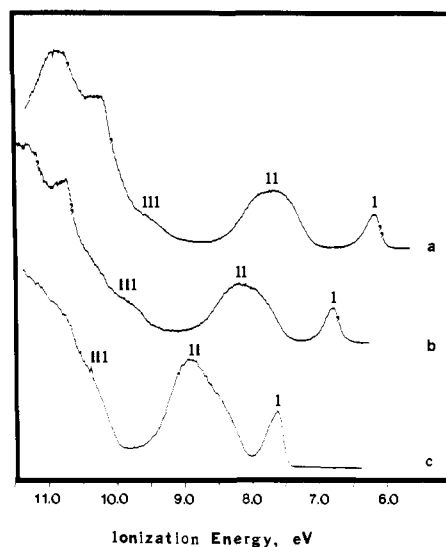
potential, easier to oxidize, than the $W_2(np)_2(O_2CEt)_4$ molecule, consistent with the higher formal oxidation state of the latter. The second oxidations occur at potentials ca. 1.0 V more positive than the first. Presumably these oxidations correlate with the successive removal of electrons from the δ orbital, resulting in valence electronic configurations of $\pi^4\delta^1$ and $\pi^4\delta^0$, respectively.

Several electrochemical studies have been reported for M_2-$(O_2CR')_4$ (M = Mo, W) complexes and all are typically dominated by oxidation chemistry.[22,55,56] In order to compare the change of metal (M = W vs. Mo) we looked at both $Mo_2(O_2CEt)_4$ and $Mo_2(np)_2(O_2CMe)_4$. These compounds, in our hands, exhibit reversible initial oxidations and irreversible second oxidations, qualitatively similar to those of the tungsten analogues. In these cases both oxidations occur at a potential 0.6 V more positive than their tungsten counterparts. This shift is precisely that expected, namely that the ditungsten compound is easier to oxidize than its dimolybdenum analogue.

The important ramification is that for molecules with filled δ orbitals as their HOMOs, the electrochemical oxidations are qualitatively similar irrespective of their d^3–d^3 or d^4–d^4 origin. With these results in mind, let us ask whether or not the ease of electrochemical oxidation correlates with the first ionization potentials in the gas phase.

Photoelectron Spectra. Since several of these complexes are readily sublimed, they are amenable to gas-phase photoelectron spectroscopic studies. As can be seen from Table XI, such studies have been restricted to the bis(neopentyl) derivatives of the alkyl carboxylate species. These provide sufficient variety for firm assignments of the various ionizations. The compounds studied were all run at their sublimation temperatures, and no signs of decomposition were observed (initial and final scans were identical).

Since the M–M quadruply bonded compounds $M_2(O_2CR')_4$ also contain the $\pi^4\delta^2$ manifold, it is appropriate to review and compare previous assignments on these systems. The $M_2(O_2CR')_4$ compounds show a relatively narrow, low-energy photoionization from the weakly bonding M–M δ orbital and a second, relatively broad, higher energy photoionization from the strongly bonding M–M π orbitals.[15,23,24,57] For $W_2(O_2CR')_4$ compounds a third narrow ionization (ca. 0.26-eV fwhm) is seen at even higher binding energy, which has been the focus of much recent attention.[25,27,58]

(53) Murray, R. W.; Reilley, C. N. *Electroanalytical Principles*; Interscience: New York, 1963.
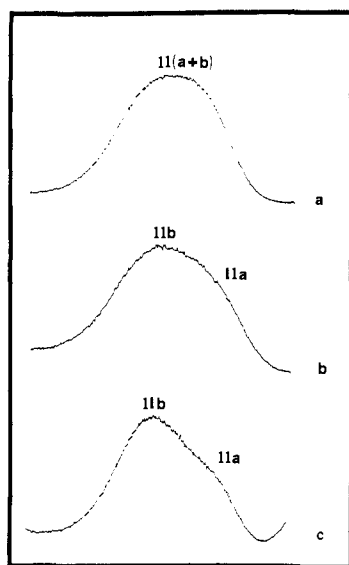(54) Nicholson, R. S. *Anal. Chem.* **1965**, *37*, 1351.

(55) Cotton, F. A.; Pedersen, E. *Inorg. Chem.* **1975**, *14*, 399.
(56) Zietlow, T. C.; Klendworth, D. D.; Nimry, T.; Salmon, D. J.; Walton, R. A. *Inorg. Chem.* **1981**, *20*, 947.
(57) Lichtenberger, D. L.; Blevins, C. H., III. *J. Am. Chem. Soc.* **1984**, *106*, 1636.

6806 *J. Am. Chem. Soc., Vol. 109, No. 22, 1987*

Chisholm et al.

Figure 13. Expanded views of the ionization labeled II in Figure 12 showing two distinct components for $W_2(np)_2(O_2CR')_4$ where R' = Me (a), H (b), and CF_3 (c).

Within the context of our current understanding of the photoelectron spectra of M–M multiply bonded complexes, this ionization can only be assigned to an ionization from an orbital that is predominantly M–M σ bonding in character (the higher energy σ orbital, $5a_{1g}$ in Figure 10).[27,59] In fact, the narrowness of this band appears to be one of the characteristic features of the σ ionization of M–M-bonded systems.[27] With this background in mind, a comparison with the photoelectron spectra of M_2R_2-$(O_2CR')_4$ complexes is most revealing, and Table XI lists the individual band positions and relative areas of the ionizations for a series of $M_2(O_2CR')_4$ and $M_2R_2(O_2CR')_4$ compounds based on a comparison of the d^3–d^3 and d^4–d^4 complexes.

The higher energy ionizations (>11 eV) of $M_2R_2(O_2CR')_4$ complexes are essentially a summation of the bands observed for the analogous $M_2(O_2CR')_4$ species[15,23–25] plus two np groups[60,61] and will not be discussed further. The lower energy ionizations, which tend to be from orbitals with substantial metal character, are most interesting. Close-ups of this region for three complexes $W_2(np)_2(O_2CR')_4$, where R' = Me, H, CF_3, are shown in Figure 12. The intense bands starting at 10–11 eV can be readily assigned to ionizations from the carboxylate ligands, presumably from their highest lying π orbitals. To lower energy, the complexes exhibit three similar features, which are designated I, II, and III in Figure 12. The lowest energy ionization (I) is seen to be quite sharp (fwhm <0.3 eV) and is followed by a second, broader ionization at 1.0–1.5-eV higher energy (II). The misshapen appearance of this latter band implies the presence of more than one component. This observation is made more apparent when the widths of these bands are compared to the analogous bands of $W_2(O_2CR')_4$ complexes as shown in Table XI. A third feature (III) is observed as a shoulder on the side of the carboxylate-based ionizations. The relative shifts of these three features can be readily attributed to the inductive effects of the O_2CR' groups, and similar shifts were previously observed in the spectra of $M_2(O_2CR')_4$ compounds.[15,23–25]

(58) (a) Sattelberger, A. P. In *Inorganic Chemistry: Towards the 21st Century*; Chisholm, M. H., Ed.; American Chemical Society: Washington, DC, 1983; pp 291–300. (b) Lichtenberger, D. L. *Ibid.*, p 301. (c) Lichtenberger, D. L. *Abstracts of Papers*, 187th National Meeting of the American Chemical Society, St. Louis, MO; American Chemical Society: Washington, DC, 1984; INOR 48.

(59) Root, D. R.; Blevins, C. H.; Lichtenberger, D. L.; Sattelberger, A. P.; Walton, R. A. *J. Am. Chem. Soc.* **1986**, *108*, 953.

(60) Evans, S.; Green, J. C.; Joachin, P. J.; Orchard, A. F.; Turner, D. W.; Maier, J. P. *J. Chem. Soc., Faraday Trans. 2* **1972**, *68*, 905.

(61) Lappert, M. F.; Pedley, J. B.; Sharp, G. *J. Organomet. Chem.* **1974**, *66*, 271.
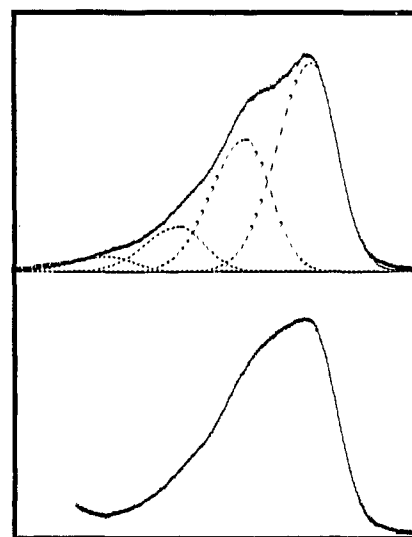
Figure 14. Expanded view of the first ionizations (feature I in Figure 12) representing removal of an electron from the δ orbital in $W_2(O_2CCF_3)_4$ (top) and $W_2(np)_2(O_2CCF_3)_4$ (bottom). The top spectrum was taken from C. H. Blevins, Ph.D. Dissertation, University of Arizona.

Ionization Energy, eV
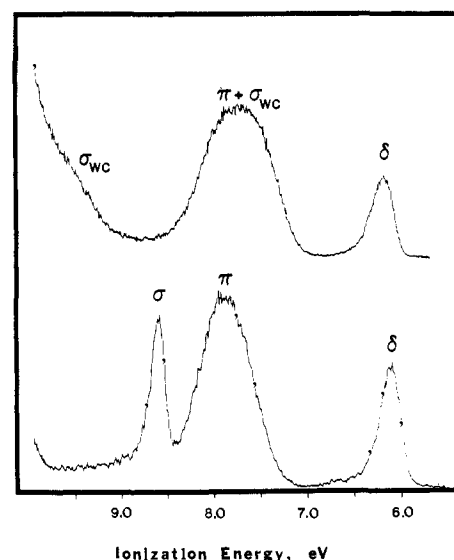
Figure 15. Comparison of the upper valence photoelectron spectra, He(I), of $W_2(np)_2(O_2CMe)_4$ (top) and $W_2(O_2CMe)_4$ (bottom).

Expanded views of feature II for $W_2(np)_2(O_2CR')_4$, where R' = Me, H, and CF_3, are shown in Figure 13. It is reasonably clear from Figure 13 that two ionizations are really present in feature II, and these are designated IIa and IIb. Bigaussian analysis of the band shapes suggests both peaks IIa and IIb are rather broad (fwhm ca. 0.6 eV).

Detailed comparisons of the $W_2(np)_2(O_2CR')_4$ spectra with those of the closely related $W_2(O_2CR')_4$[25,62] compounds are quite revealing. In Figure 14, feature I of $W_2(np)_2(O_2CCF_3)_4$ is compared to the first ionization band of $W_2(O_2CCF_3)_4$, which has been assigned to the removal of an electron from the M–M δ bond.[25,62,63] The two spectra are essentially identical, having the same narrow width (Table XI) and the same vibrational progression ($\hbar\omega$ = 1000 cm^{-1}; C–F stretch). Close-up comparisons of the spectra of the O_2CMe analogues are also essentially identical with one another, and it is thus implied that feature I in $W_2R_2(O_2CR')_4$ compounds arises from ionization of a M–M δ-bonding electron.

In Figure 15, the upper valence region of $W_2(np)_2(O_2CMe)_4$

(62) Sattelberger, A. P.; Lichtenberger, D. L.; Blevins, C. H., III, results to be published.
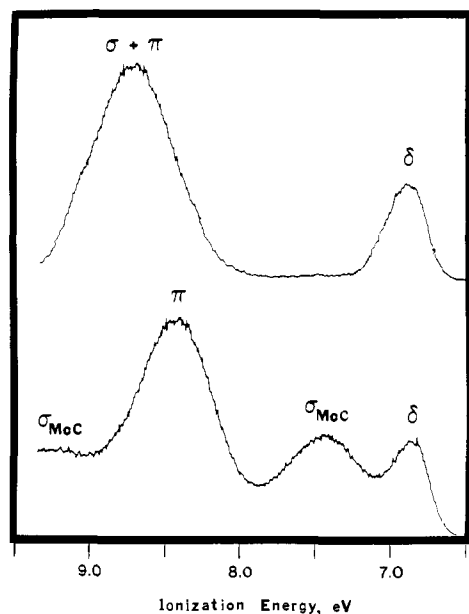
Figure 16. Comparison of the upper valence photoelectron spectra, He(I), for $Mo_2(O_2CMe)_4$ (top) and $Mo_2(np)_2(O_2CMe)_4$ (bottom).

is compared to this same region of $W_2(O_2CMe)_4$ in which the first three ionization bands have been assigned to M—M δ-, π-, and σ-orbital ionizations, respectively.[25,27,62,63] This comparison is meant to illustrate several very important points: (i) that ionization from a M—M δ bond is readily assigned to feature I, (ii) that an ionization from a M—M π bond could be present as one of the components of feature II, and (iii) that the narrow ionization assigned to the M—M σ bond of $W_2(O_2CR')_4$ is either not present in feature II or it has been dramatically changed in character.

Finally, it should be noted that feature III has no analogue in the spectra of $W_2(O_2CR')_4$ compounds. Careful examination of feature III showed it to be consistently reproducible despite the problem of a rising background in this spectral region. Similar studies of $W_2(O_2CR')_4$ complexes clearly showed the absence of such a feature, as background subtraction revealed a lack of intensity between the M—M σ and π ionizations and the onset of the carboxylate-based bands. This aspect of the spectra can be observed in Figure 15.

Confirmation of these assessments and assignments is found in the comparison of the photoelectron spectra of $Mo_2(O_2CMe)_4$ and $Mo_2(np)_2(O_2CMe)_4$ (Figure 16). The spectrum of $Mo_2(np)_2(O_2CMe)_4$ clearly shows four ionization bands, as were argued to be present for the tungsten analogue. The first two ionizations in the spectrum of $Mo_2(O_2CMe)_4$ have been assigned as originating from the M—M δ and π orbitals, respectively,[15,23,24,57] but the location of the ionization from a M—M σ orbital is still unclear. Comparison of the peak shapes and intensities strongly suggests that the first and third ionization bands of $Mo_2(np)_2$-$(O_2CMe)_4$ correspond to the δ and π ionizations, respectively.

Several trends regarding the peak positions listed in Table XI support this assignment of the δ and π bond ionizations. First, the separation between the δ and π ionizations is fairly constant at ca. 1.5 eV, and this pattern has been firmly established for the $M_2(O_2CR')_4$ species. Since the $W_2(np)_2(O_2CR')_4$ analogues have nearly identical metal—metal distances, it would be logical to expect that a similar δ—π separation would result. Second, the metal-centered ionizations all shift by ca. 0.3 eV to higher binding energy in going from $W_2(O_2CR')_4$ to $W_2(np)_2(O_2CR')_4$. This observation is consistent with the metal being in a higher formal oxidation state and similar coordination environment and parallels the electrochemical data. In comparing the δ ionizations from the $Mo_2(O_2CMe)_4$ and $Mo_2(np)_2(O_2CMe)_4$ compounds, we note that the ionization from the Mo_2^{6+}-containing compound is at slightly

lower energy. Presumably this reflects the lengthening of the Mo—Mo bond, which opposes the effect of increased charge described above. Third, the metal-centered ionizations shift by more than 0.5 eV to higher binding energy in going from W to Mo. This reflects the general trend that second-row early transition metals in mid to high oxidation states are harder to oxidize than their third-row counterparts. This was also previously observed in the electrochemistry.

Given the similarities in band shapes and the rational trends in band positions, it is difficult to dispute the proposed assignments of the δ and π ionization bands. On the basis of this ionization data, it must be concluded that the $M_2(np)_2(O_2CR')_4$ species have the valence M—M $\pi^4\delta^2$ configuration.

The remaining two bands which are most pronounced in the $Mo_2(np)_2(O_2CMe)_4$ spectrum are then ascribed to ionizations from orbitals that are primarily M—C σ bonding, since their absence in the spectra of $M_2(O_2CR')_4$ species discourages any assignment relating to that framework. Both ionizations appear to be broad (fwhm ca. 0.6 eV) and occur in the region 8–10 eV, which is typical of M—C σ bond ionizations.[60,61]

A final comment concerns the narrow ionization at 8.6 eV in the spectrum of $W_2(O_2CR')_4$ compounds and the absence of an analogous peak in the $W_2(np)_2(O_2CR')_4$ spectra. The origin of this sharp peak has been the subject of debate,[58] though it is now rather firmly assigned to ionization from the M—M σ bond.[25,27] Alternative assignments that have been proposed are (1) that it is a component of the π bond ionization split out by spin—orbit coupling[64] or (2) that it represents a non-Koopman's state ($\sigma^2\pi^4\delta^*$ configuration) formed from a δ bond ionization.[58b,c] Why the mechanisms proposed in the two alternative assignments would not be operating for the present complexes is not at all obvious. Actually, the absence of this sharp band in the spectra of W_2-$(np)_2(O_2CR')_4$ compounds, which have the $\pi^4\delta^2$ configuration, confirms its assignment to a M—M σ bond ionization. The summation of all the various ionization data makes a rather tight argument for the assignments of the M—M σ, π, and δ type ionizations in the two series of compounds $M_2R_2(O_2CR')_4$ and $M_2(O_2CR')_4$.

Let us then turn our attention briefly to the calculated ionization energies as determined by the relativistic $X\alpha$—SW method. For the model compound of formula $W_2(O_2CH)_4$, the relativistic $X\alpha$—SW method places the π ionization at 1.99 eV higher binding energy than δ, in good quantitative agreement with the experimental δ—π separations of 1.91, 1.77, and 1.76 eV for $W_2(O_2CR')_4$, where R' = C(CH$_3$)$_3$, CH$_3$, and CD$_3$, respectively. However, the calculations place the first σ ionization (from the $5a_{1g}$ orbital) 2.3 eV below the π ionization. This is, in fact, a general observation in that the $X\alpha$—SW calculations on M—M quadruply bonded systems *always* place the σ orbitals well below the π orbitals. By contrast, Ziegler's relativistic Hartree—Fock—Slater (DV-$X\alpha$) calculation[63] on $W_2(O_2CCF_3)_4$ yields a δ—π splitting of 1.15 eV, which is rather small, but yields a σ—π splitting of 0.6 eV, in good agreement with the experimental results. Similarly, $X\alpha$—SW calculations[17] on $Mo_2(O_2CH)_4$ give a σ—π splitting on the order of 1.0 eV, whereas recent DV-$X\alpha$ calculations[65] on the same molecule predict the σ and π ionizations to be isoenergetic, a result also obtained with multiconfiguration ab initio methods.[66] It thus appears that discrete variational and scattered wave solutions to the $X\alpha$ method differ with respect to the placement of the σ orbital in $M_2(O_2CH)_4$ (M = Mo, W) compounds. We believe that the inability of the $X\alpha$—SW method to properly place the σ orbitals is due to some of the assumptions of the overlapping-sphere formalism, which is the accepted practice for such calculations. For these very short metal—metal bonds, the atomic spheres of the metal atoms overlap substantially, and the largest errors in the description of the M—M interaction are expected to occur for

(63) Ziegler, T. *J. Am. Chem. Soc.* **1985**, *107*, 4453.

(64) Cotton, F. A.; Hubbard, J. L.; Lichtenberger, D. L.; Shim, I. *J. Am. Chem. Soc.* **1982**, *104*, 679.

(65) Manning, M. C.; Holland, G. F.; Ellis, D. E.; Trogler, W. C. *J. Phys. Chem.* **1983**, *87*, 3083.

(66) Atha, P. M.; Hillier, I. H.; Guest, M. F. *Mol. Phys.* **1982**, *46*, 437.

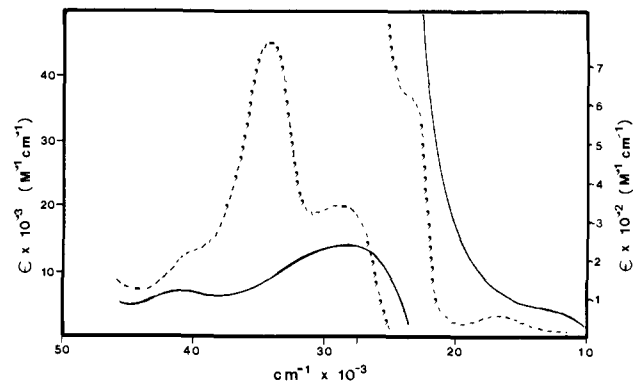6808 *J. Am. Chem. Soc., Vol. 109, No. 22, 1987*

Chisholm et al.
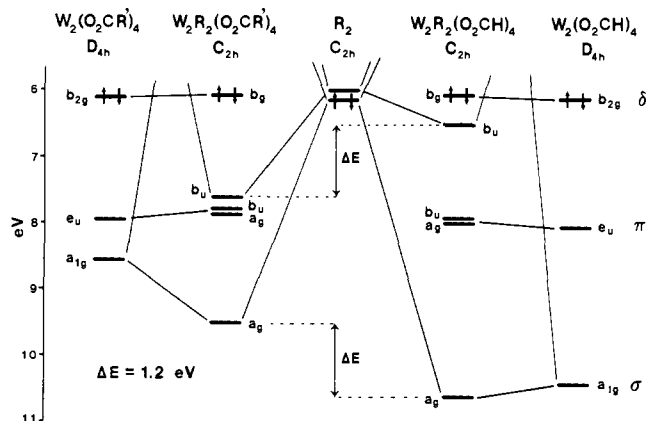
Figure 17. Qualitative interaction diagram comparing the experimental (left two columns) and calculated (right two columns) electronic structure of $W_2(O_2CR')_4$ and $W_2R_2(O_2CR')_4$ complexes. This diagram illustrates qualitatively the difference between experimental and calculated energies of σ type orbitals, represented by ΔE.

Figure 18. Comparison of the electronic absorption spectra of W_2-$(np)_2(O_2CEt)_4$ (dashed line) and $W_2(O_2CEt)_4$ (solid line) in the region 10000–50000 cm^{-1} recorded in hexane at room temperature.

Figure 19. Comparison of the electronic absorption spectra of Mo_2-$(O_2CMe)_4$ (solid line) and $Mo_2(np)_2(O_2CMe)_4$ (dashed line) in the region 10000–45000 cm^{-1} recorded in CH_2Cl_2 at room temperature.

those orbitals that have their maximum interatomic interactions in the overlap region. This will not be a problem for the δ and π orbitals, but could be (and apparently is) for the σ orbitals.[67] The DV–Xα method, which does not employ the scattered-wave method of solution, is apparently able to model the M–M σ interaction more accurately.

For the model compound of formula $W_2(O_2CH)_4(CH_3)_2$ the relativistic Xα–SW method places the π ionization at 1.84 eV higher binding energy than δ, which is again in good quantitative agreement with the experimental δ–π separations of ca. 1.5 eV. Perhaps more important is that the Xα calculation predicts that ionization from a W–C σ-bonding orbital ($15b_u$) should lie between the δ and π ionizations, which is in excellent agreement with the experimental results.

The relativistic Xα–SW calculations, despite shortcomings, have helped us to arrive at a consistent correlation of the PES and bonding in $W_2(O_2CR')_4$ and $W_2R_2(O_2CR')_4$ complexes. We have attempted to correlate all of the information available from the PES and calculations and construct a qualitative interaction diagram. This diagram, shown in Figure 17, was constructed by using the PES peak energies and assignments to fix the positions of the levels of $W_2(O_2CMe)_4$ and $W_2(np)_2(O_2CMe)_4$ which correspond to the ground-state electronic structure for the two species. The a_g and b_u levels of $(np)_2$ were taken to be isoenergetic with the b_{2g}, δ-bonding orbital, in parallel wih the Xα–SW results. Only the occupied levels are shown. We believe that this diagram accounts *qualitatively* for the important features in the PES and provides us with a simple basis for comparison of observed and calculated results. It is readily seen from this figure that the calculation is off with respect to the orbitals of σ symmetry, as previously discussed, and that the magnitude of error can be represented as the quantity ΔE. This may in fact be related to Ziegler's exchange repulsion energy,[63,68] the quantity that is apparently underestimated in the scattered-wave solution. It is interesting to note that Ellis[65] and Ziegler[68] have independently predicted that the metal-localized σ level is actually destabilized at shorter internuclear distances in two very different quadruply bonded systems: $Mo_2(O_2CH)_4$ and $M_2X_4(PR_3)_4$ (where M = Cr, Mo, and W). This extreme sensitivity of the σ-orbital energies to relatively small perturbations may partially explain the discrepancy among the various theoretical predictions of the PES of quadruply bonded transition-metal systems.[65]

Electronic Absorption Spectra. For molecules with M–M quadruple bonds the most studied and perhaps most fascinating
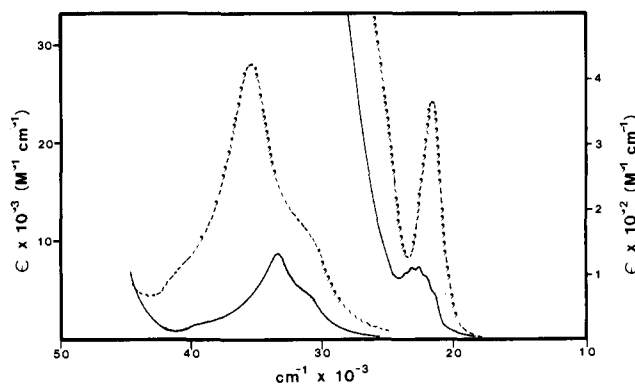
feature of the electronic absorption spectra is the $^1A_{1g} \rightarrow {}^1A_{2u}$ ($\delta \rightarrow \delta^*$) transition.[2] Historically there was a great deal of controversy involved in the assignment of the $\delta \rightarrow \delta^*$ transition as the lowest energy transition in $Mo_2(O_2CR')_4$ species.[17-20] There appeared to be no band that could be assigned to this transition until 1979, when Martin, Newman, and Fanwick provided the definitive explanation for the assignment of this transition to a 23000-cm^{-1} absorption feature.[21] A detailed review of the historical problem and ultimately the results that allowed for the assignment was published by Martin in 1982.[69]

Much more recently the electronic spectra of $W_2(O_2CR')_4$ species have been reported by Cotton (R′ = Ar)[41] and Sattelberger (R′ = alkyl).[22] Sattelberger has presented arguments for the assignment of the lowest energy electronic absorption bands in $W_2(O_2CCF_3)_4$ and $W_2(O_2CCMe_3)_4$ spectra to the spin-forbidden $\delta \rightarrow \delta^*$ ($^1A_{1g} \rightarrow {}^3A_{2u}$) transition. The authors argue that the spin-allowed $\delta \rightarrow \delta^*$ ($^1A_{1g} \rightarrow {}^1A_{2u}$) transition in these molecules is completely "masked" by the intense $\delta \rightarrow \pi^*_{(oco)}$ MLCT transition. A comparison of the spectra for $M_2(O_2CR')_4$ and $M_2R_2(O_2CR')_4$ compounds proves very informative with regard to spectral assignments for the new d^3–d^3 compounds and clarifies previous speculations concerning the spectra of the d^4–d^4 carboxylates. Absorption maxima and molar extinction coefficients are given in Table XII for $M_2(O_2CR')_4$ and $M_2R_2(O_2CR')_4$ compounds of structural type I.

The $\delta \rightarrow \delta^*$ Transition. Figure 18 shows the room-temperature electronic absorption spectra of $W_2(O_2CEt)_4$ and $W_2(np)_2$-$(O_2CEt)_4$ obtained from hexane solutions in the range 1000–220 nm. Figure 19 shows the spectra of $Mo_2(O_2CMe)_4$ and Mo_2-$(np)_2(O_2CMe)_4$, and Figure 20 provides a comparison of the

(67) Sattelberger and Scioly have found that the Xα–SW energies of the σ orbitals of $W_2(O_2CH)_4$ are extremely sensitive to the choice of sphere radii, consistent with this conjecture. See: Scioly, A. J. Ph.D. Thesis, University of Michigan, 1985.

(68) Ziegler, T. *J. Am. Chem. Soc.* **1984,** *106,* 5901.

(69) Martin, D. S.; Newman, R. A.; Fanwick, P. E. *Inorg. Chem.* **1982,** *21,* 3400.
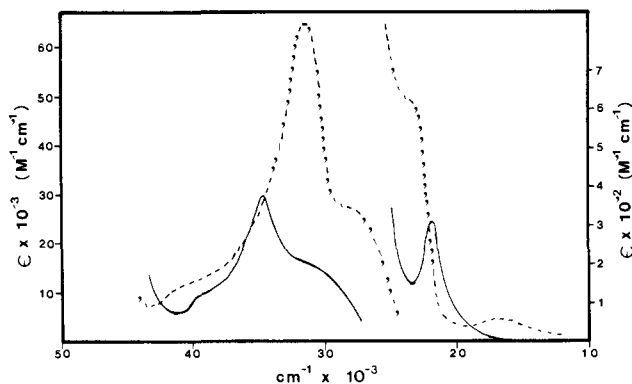
Figure 20. Comparison of the electronic absorption spectra of M_2-$(np)_2(O_2CMe)_4$ where the solid line represents that for M = Mo and the dashed line that for M = W. Spectra were recorded in CH_2Cl_2 at room temperature.

spectra for $M_2(np)_2(O_2CMe)_4$ compounds where M = Mo and W.

The first observation germane to the electronic spectra of compounds of structural type I is that the spectra of Mo_2-$(O_2CMe)_4$[70] and $Mo_2(np)_2(O_2CMe)_4$ shown in Figure 19 are remarkably similar. Indeed, we note that the singlet $\delta \rightarrow \delta^*$ transition (23 000 cm^{-1}, ϵ = 150 M^{-1} cm^{-1}) of $Mo_2(O_2CMe)_4$ is red-shifted by only 1200 cm^{-1} in the $Mo_2(np)_2(O_2CMe)_4$ spectrum (21 800 cm^{-1}, ϵ = 320 M^{-1} cm^{-1}). This observation establishes the fact that the singlet $\delta \rightarrow \delta^*$ transition in structural type I complexes of molybdenum occurs at approximately the same energy. The small red shift is consistent with the slight lengthening (ca. 0.04 Å) in the Mo–Mo distance as a consequence of the axial alkyl ligands. Thus, in the type I compounds of tungsten, where the W–W distance is virtually identical, one might expect to see the $\delta \rightarrow \delta^*$ transition at about the same energy for both W_2R_2-$(O_2CR')_4$ and $W_2(O_2CR')_4$ complexes.

Examination of the electronic spectra of the ditungsten compounds shows that both species exhibit a weak ($\epsilon \sim 30$ M^{-1} cm^{-1}) absorption feature near 16 000 cm^{-1}. An intense absorption ($\epsilon \sim 13 000$ M^{-1} cm^{-1}) at ca. 28 000 cm^{-1} in the spectra of W_2-$(O_2CR')_4$ compounds is blue-shifted by about 1000 cm^{-1} in the $W_2R_2(O_2CR')_4$ spectra, uncovering a distinct shoulder near 23 000 cm^{-1} which is not observed in the $W_2(O_2CR')_4$ spectra.[22]

At this point we can glean some valuable information from the transition energies as calculated via the relativistic Xα–SW technique.[44] The relativistic Xα–SW calculations performed in our laboratories predict that the lowest energy electronic transition in both species should be the $\delta \rightarrow \delta^*$ transition. The calculated transition energies for the $\delta \rightarrow \delta^*$ transition are 12 500 and 12 800 cm^{-1} for the model compounds $W_2(O_2CH)_4$ and $W_2(CH_3)_2(O_2$-$CH)_4$, respectively. The lowest energy experimental transition is observed near 16 000 cm^{-1}, which is remarkably close to the calculated value. In fact, the experimental and calculated values are *much too close*. It is known that even with the inclusion of relativistic corrections, the $\delta \rightarrow \delta^*$ transition energy calculated by the Xα–SW method is generally too low by a factor of 2.[71] For example, it is generally agreed that the $\delta \rightarrow \delta^*$ transition for $Re_2Cl_8^{2-}$ occurs at ca. 14 000 cm^{-1},[72] whereas the calculated

transition energy based on the relativistic Xα–SW method is only 7040 cm^{-1}.[72] Thus, in view of our current understanding and previous workers' findings based on the Xα–SW method, the lowest energy transition at ca. 16 000 cm^{-1} in both $W_2R_2(O_2CR')_4$ and $W_2(O_2CR')_4$ complexes is much too close to the calculated value of 12 500 cm^{-1} to be the spin-allowed $\delta \rightarrow \delta^*$ transition. In fact, if our calculated $\delta \rightarrow \delta^*$ energy is the same *percentage* of the experimental energy as other workers have found, then the experimental band should lie near 25 000 cm^{-1} (2 × 12 500 cm^{-1}). In light of this discussion, the most reasonable candidate for the singlet $\delta \rightarrow \delta^*$ transition is the 23 000-cm^{-1} shoulder observable in the spectra of $W_2R_2(O_2CR')_4$ species. The intense MLCT transition (vide infra) is shifted ca. 1000 cm^{-1} to lower energy in $W_2(O_2CR')_4$ compounds and has apparently "masked" the $\delta \rightarrow \delta^*$ ($^1A_{1g} \rightarrow {}^1A_{2u}$) transition in this species. Figure 18 demonstrates this phenomenon rather nicely.

Thus far we have only presented arguments based on the calculated transition energies. Sattelberger and Santure have proposed essentially the same assignments for $M_2(O_2CR')_4$ complexes based on comparisons with other Mo and W complexes,[22] and we feel that our studies on the $M_2R_2(O_2CR')_4$ complexes both complement and reinforce their proposals.

It is instructive to review some of the other arguments against assigning the lowest energy transition to the spin-allowed $\delta \rightarrow \delta^*$ transition. (1) Hay demonstrated that the highly localized nature of the δ orbitals in the ground state leads to decreased orbital overlap and hence the intrinsically low intensity of the $\delta \rightarrow \delta^*$ transition in dinuclear quadruply bonded transition-metal complexes.[73] (2) Trogler and Manning have observed an increase in the intensity of the $\delta \rightarrow \delta^*$ transition for $M_2(mhp)_4$ and $M_2Cl_4(PR_3)_4$ complexes (M = Cr, Mo, and W; mhp = the anion derived from 2-methyl-6-hydroxypyridine) upon going from first- to third-row metals.[74] They suggested that a descent in the periodic table leads to larger metal d orbitals and hence better δ overlap, resulting in an increased $\delta \rightarrow \delta^*$ intensity. Thus, one would expect the intensity of the $\delta \rightarrow \delta^*$ ($^1A_{1g} \rightarrow {}^1A_{2u}$) transition to increase from Mo to W. The intensities ($\epsilon \sim 30$ M^{-1} cm^{-1}, $f \sim 10^{-4}$) of the 16 000-cm^{-1} absorption features in spectra of W-containing type I compounds are an order of magnitude weaker than the intensities of the $\delta \rightarrow \delta^*$ transitions in $Mo_2(O_2CR')_4$ spectra ($\epsilon \sim 150$ M^{-1} cm^{-1}, $f \sim 10^{-3}$). Other pertinent arguments may be found in the paper by Sattelberger and Santure.[22]

In view of the above and the calculated transition energies, the lowest energy electronic transition in the spectra of $W_2(O_2CR')_4$ and $W_2R_2(O_2CR')_4$ complexes is both too low in energy and too weak in intensity to be the spin-allowed $\delta \rightarrow \delta^*$ transition. Again, we reach the inescapable conclusion that the most likely candidate for the spin-allowed $\delta \rightarrow \delta^*$ transition in the $W_2R_2(O_2CR')_4$ spectra is the shoulder at ca. 23 000 cm^{-1} ($\epsilon \sim 600$ M^{-1} cm^{-1}). This is about the same energy as the $\delta \rightarrow \delta^*$ transition in Mo_2-$(O_2CR')_4$ spectra and its intensity is increased relative to Mo as expected. Thus, we propose that for both $W_2(O_2CR')_4$ and $W_2R_2(O_2CR')_4$ compounds, the lowest energy transition at ca. 16 000 cm^{-1} ($\epsilon \sim 1$–30 M^{-1} cm^{-1}) is the spin-forbidden $\delta \rightarrow \delta^*$ transition ($^1A_{1g} \rightarrow {}^3A_{2u}$ in D_{4h}, $^1A_g \rightarrow {}^3B_u$ in C_{2h}), and that the spin-allowed $\delta \rightarrow \delta^*$ transition ($^1A_{1g} \rightarrow {}^1A_{2u}$ and $^1A_g \rightarrow {}^1B_u$, respectively) is ca. 9000 cm^{-1} higher in energy at ca. 23 000 cm^{-1}, observable for $W_2R_2(O_2CR')_4$ compounds but not for $W_2(O_2CR')_4$ compounds.

In Figure 20 we show a comparison of solution spectra of $M_2(np)_2(O_2CMe)_4$, where M = Mo and W. For the Mo-containing compound, the spin-allowed $\delta \rightarrow \delta^*$ transition appears at 21 800 cm^{-1} (ϵ = 320 M^{-1} cm^{-1}). For the W analogue, the proposed spin-allowed $\delta \rightarrow \delta^*$ transition actually appears at slightly higher energy (ca. 23 000 cm^{-1}) with an increased intensity (ϵ = 600 M^{-1} cm^{-1}) as expected, in support of our view that the spin-allowed $\delta \rightarrow \delta^*$ transition for type I complexes of Mo and

(70) It is interesting to note that vibrational fine structure in the $\delta \rightarrow \delta^*$ transition of $Mo_2(O_2CMe)_4$ is observed even at room temperature under our experimental conditions. See ref 2.

(71) See, for example: (a) Cowman, C. D.; Gray, H. B. *J. Am. Chem. Soc.* **1973**, *95*, 8177. (b) Cowman, C. D.; Trogler, W. C.; Gray, H. B. *Isr. J. Chem.* **1976**, *15*, 308. (c) Sattelberger, A. P.; Fackler, J. P. *J. Am. Chem. Soc.* **1977**, *99*, 1258. (d) Fanwick, P. E.; Martin, D. S.; Cotton, F. A.; Webb, T. R. *Inorg. Chem.* **1977**, *16*, 2103. (e) Bursten, B. E.; Clark, D. L. *Polyhedron* **1987**, *6*, 695. See also ref 18 and 21.

(72) Bursten, B. E.; Cotton, F. A.; Fanwick, P. E.; Stanley, G. S. *J. Am. Chem. Soc.* **1983**, *105*, 3082. For [$Mo_2Cl_8^{4-}$] the observed and calculated energies are 18 000 and 9200 cm^{-1}, respectively. See: Norman, J. G., Jr.; Kolari, H. J.; Gray, H. B.; Trogler, W. C. *Inorg. Chem.* **1977**, *16*, 987.

(73) Hay, P. J. *J. Am. Chem. Soc.* **1982**, *104*, 7007. See also: Trogler, W. C.; Gray, H. B. *Acc. Chem. Res.* **1978**, *11*, 232, and ref 2.

(74) Manning, M. C.; Trogler, W. C. *J. Am. Chem. Soc.* **1983**, *105*, 5311 and references therein.

Table XII. Electronic Absorption Data for $W_2(O_2CR')_4$ and $W_2R_2(O_2CR')_4$ Molecules

compd	solvent	λ, nm	λ, cm⁻¹	ε, M⁻¹ cm⁻¹	ref
$W_2(O_2CCF_3)_4$	THF	688	14500	1.7	22
		426 sh	23500		
		395	25300	15000	
	CH_2Cl_2	600 sh	16700	13	a
		413 sh	24200	10000	
		388	25700	14000	
		365 sh	27400	11000	
		302	33100	2300	
		270	37000	3200	
		253	39500	5500	
$W_2(O_2CMe_3)_4$	THF	735	13600	1.0	22
		377	26500	13000	
$W_2(O_2CEt)_4$	hexane	700 sh	13000	60	a
		357	27000	13000	
		242	41000	2900	
$W_2(O_2CC_6H_5)_4$	THF	590	16800		41
		549	18200		
	toluene	560	17900		41
		520	19200		
	CH_2Cl_2	551	18100	10000	a
		518	19300	10000	
		365	27500	30000	
		276	36200	40000	
		268	37300	40000	
		231	43300	60000	
	THF	598	16700	10000	a
		559	17900	10000	
		345	29000	30000	
		282	35500	40000	
		275	36400	40000	
		239	41900	60000	
$W_2(O_2CC_6H_4\text{-}4\text{-}OCH_3)_4$	THF	580	17200		41
		549	18500		
	toluene	550	18200		41
		508	19700		
	CH_2Cl_2	554	18100	10000	a
		551	18200	10000	
		410 sh	24400	4000	
		363 sh	27500	3000	
		282 sh	35500	40000	
		273 sh	36600	40000	
		268	37300	40000	
$W_2(O_2CC_6H_2[2,4,6\text{-}CH_3]_3)_4$	THF	664	15100		41
		477	21000		
		400	25000		
	toluene	466	21500		41
$PhCO_2H$	cyclo-hexane	282	35500		b
		272	36800		
		230	43500		
$W_2(np)_2(O_2CEt)_4$	hexane	600	16700	170	a
		436 sh	22900	600	
		341	29300	18000	
		293	34100	45000	
		257 sh	38900	13000	
		251 sh	39800	11000	
		245 sh	40800	10000	
		239 sh	41800	9300	

compd	solvent	λ, nm	λ, cm⁻¹	ε, M⁻¹ cm⁻¹	ref
$W_2(np)_2(O_2CCH_3)_4$	CH_2Cl_2	585	17100	29	a
		435 sh	23000	660	
		357	28000	15000	
		318	31500	65000	
$W_2(np)_2(O_2CH)_4$	CH_2Cl_2	550	18200	21	a
		441 sh	22700	710	
		334	29900	13000	
		293	34100	42000	
		250 sh	40000	9200	
$W_2(np)_2(O_2CCF_3)_4$	hexane	500 sh	20000	82	a
		440 sh	22700	990	
		360 sh	27800	16000	
		301	33200	47000	
		245 sh	40800	8300	
$W_2(np)_2(O_2CC_6H_5)_4$	CH_2Cl_2	620 sh	16100	160	a
		509 sh	19600	31000	
		482	20700	33000	
		450 sh	22200	25000	
		357	28000	2500	
		295	33900	31000	
		279	35800	27000	
		273	36600	22000	
		242	41300	33000	
	THF	619 sh	16200		a
		505 sh	19200		
		477	21000		
		450 sh	22200		
		345	29000		
		293	34100		
		278	36000		
		270	37100		
		243	41200		
$W_2(np)_2(O_2CC_6H_4\text{-}4\text{-}OMe)_4$	CH_2Cl_2	610 sh	16400	170	a
		510 sh	19600	35000	
		484	20700	38000	
		451 sh	22200	31000	
		355 sh	28200	5200	
		296	33800	43000	
		276	36200	84000	
		270	37000	82000	
$W_2(np)_2(O_2CC_6H_2[2,4,6\text{-}Me_3])_4$	THF	595	16800	74	a
		408	24500	25000	
		298	33600	35000	
$W_2Me_2(O_2CPh)_4$	CH_2Cl_2	490 sh	20400	20000	a
		466	21500	23000	
		435 sh	23000	18000	
		365 sh	27400	4300	
		280 sh	35700	27000	
		264	37900	37000	
$Mo_2(np)_2(O_2CMe)_4$	CH_2Cl_2	463	21600	370	a
		325 sh	30800	12000	
		285	35100	28000	
		245 sh	40800	1800	
$Mo_2(O_2CMe)_4$	EtOH/MeOH	436	22900	300	17
		324 sh	30800	6000	
		305	32800	7200	
		225	44400	2000	

a This work. *b* Pavia, D. L.; Lampman, G. M.; Kriz, G. S. *Introduction to Spectroscopy: A Guide for Students of Organic Chemistry*; W. B. Saunders: Philadelphia, 1979.

W actually occurs at about the same energy.

In the hope of providing more definitive experimental data in support of these assignments, we have examined single-crystal spectra of $W_2(np)_2(O_2CEt)_4$ at 5 K. Unfortunately, even at 5 K no vibrational fine structure is observed under our experimental conditions. However, the triplet transition is well resolved at this temperature, which establishes it as a real feature as is shown in Figure 21.

We note that a triplet δ → δ* transition has not been observed for any $Mo_2(O_2CR')_4$ species but that evidence for this transition has been presented for $Re_2(O_2CMe_3)_4Cl_2$.[75] For heavy atoms such as W or Re, the effects of spin–orbit coupling become significant and can contribute to the intensity of spin-forbidden transitions.[76] A slight mixing of singlet character into a triplet state or a mixing of triplet character into the ground state will contribute to the intensities of singlet–triplet transitions. Vibronic mixing mechanisms may be equally important for enhancing the intensities of spin-forbidden transitions.[76]

MLCT Transitions. The next feature common to both species is an intense (ε ∼ 13000 M⁻¹ cm⁻¹) absorption at 27000–29000 cm⁻¹. This band has been proposed to arise from the δ → π*$_{(oco)}$ ($^1A_{1g}$ → ^1E_u), dipole-allowed, metal-to-ligand charge-transfer (MLCT) excitation in $M_2(O_2CR')_4$ compounds of Mo[17] and W.[22]

(75) The ^{3}(δ → δ*) transition was observed in the single-crystal spectrum of $Re_2(O_2C\text{-}t\text{-}Bu)_4Cl_2$ at 16500 cm⁻¹ while the spin-allowed ^{1}(δ → δ*) was observed at 20600 cm⁻¹. See: Martin, D. S.; Huang, H.; Newman, R. A. *Inorg. Chem.* **1984**, *23*, 699.

(76) See, for example: (a) Figgis, B. N. *Introduction to Ligand Fields*; Wiley: New York, 1966. (b) Lever, A. B. P. *Inorganic Electronic Absorption Spectra*; Elsevier: Amsterdam, New York, 1984.
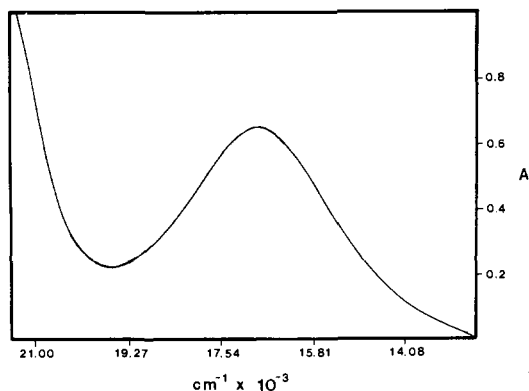
Tungsten-Tungsten Triple Bond. 13

J. Am. Chem. Soc., Vol. 109, No. 22, 1987 6811

Figure 21. Expanded view of the $^3(\delta \rightarrow \delta^*)$ transition of a single crystal of $W_2(np)_2(O_2CEt)_4$ at 5 K.
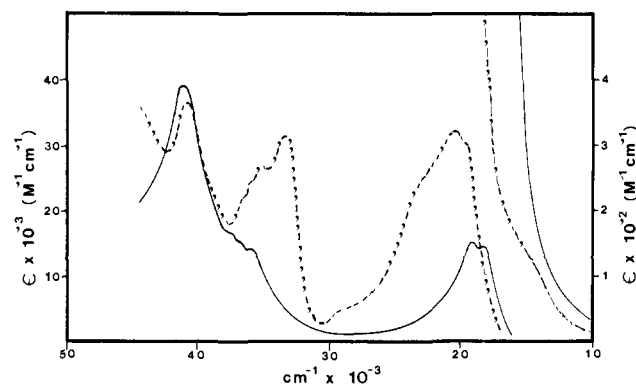

Figure 22. Comparison of the electronic absorption spectra of W_2-$(O_2CPh)_4$ (solid line) and $W_2(np)_2(O_2CPh)_4$ (dashed line) in CH_2Cl_2 solution at room temperature.

This assignment is consistent with the R group dependence of the transition energy and the high oscillator strength (see Table XII). Sattelberger noted that this transition red-shifts by 7400 cm^{-1} in going from $Mo_2(O_2CCMe_3)_4$ to $W_2(O_2CCMe_3)_4$.[22] A red-shift is expected for this transition since the δ level will rise in energy on going from Mo to W, while the $\pi^*_{(oco)}$ level of the carboxylate ligands should remain essentially the same. This transition is blue-shifted by ca. 1000 cm^{-1} in $W_2R_2(O_2CR')_4$ spectra and may be the result of a W_2^{6+} core as opposed to a W_2^{4+} core. Moreover, in $Mo_2(O_2CPh)_4$,[77] $W_2(O_2CPh)_4$,[41] and $W_2(np)_2(O_2CPh)_4$, where carboxylate π^* orbitals and aromatic π^* orbitals can interact, this band appears to shift dramatically to lower energy. Cotton and Wang[41] have examined the spectra of several arene-carboxylate complexes of formula $W_2(O_2CAr)_4$ and noted that when the arene ring was aligned parallel to the plane of the carboxylate ligands (as determined by X-ray crystallography), two bands were observed, but for Ar = $C_6H_2(2,4,6\text{-Me}_3)$, where the substituted phenyl rings are kept nearly 90° to the planes of the carboxylate groups, only a single band is observed at higher energy and the spectrum is virtually identical with the spectra of the recently reported alkyl carboxylates.[22,78] In that paper Cotton and Wang speculated on two possible reasons for the presence of two bands at low energy as opposed to the single $\delta \rightarrow \delta^*$ peak that was expected. The two possibilities were (1) that when two close bands were observed, one was due to the $\delta \rightarrow \delta^*$ transition and the other was due to the $\delta \rightarrow \pi^*_{(oco)}$ MLCT transition, and (2) that the presence of two bands may well be specific to the arene-carboxylate compounds in which conjugation between the phenyl or substituted phenyl groups alters the energy of the π^* ligand orbitals. The authors were in favor of the first possibility and suggested that some light could be shed on this point when the spectra of some alkyl-carboxylate compounds were obtained.[41] As we have already seen, the alkyl-carboxylate compounds reported by Sattelberger have not been all that straightforward either; however, the electronic spectra of $W_2R_2(O_2CAr)_4$ complexes are quite informative with respect to this matter.

A comparison of the electronic spectra of $W_2(O_2CPh)_4$ and $W_2(np)_2(O_2CPh)_4$ recorded in CH_2Cl_2 at room temperature is shown in Figure 22. We note that the spectrum of $W_2(O_2CPh)_4$, in our hands, is nearly identical with that reported by Cotton;[41] i.e., two bands are observed with extinction coefficients of ca. 15 000 M^{-1} cm^{-1}.[79] The important observation is that these two bands are *both* blue-shifted by ca. 2000 cm^{-1} in the $W_2(np)_2$-$(O_2CPh)_4$ spectrum and a weak ($\epsilon \sim 160$ M^{-1} cm^{-1}) but distinct shoulder near 16 000 cm^{-1} has appeared.[80] At this stage we

recognize the 16 000-cm^{-1} feature to be the triplet $\delta \rightarrow \delta^*$ transition, which is itself somewhat masked by the intense absorption of the MLCT bands. The intensity ($\epsilon \sim 30\,000$ M^{-1} cm^{-1}) together with the fact that both bands undergo a blue-shift in $W_2(np)_2(O_2CAr)_4$ spectra suggest that *both* bands are MLCT transitions which occur at such low energy (relative to their alkyl-carboxylate counterparts) that neither the singlet *nor* triplet $\delta \rightarrow \delta^*$ transitions are observable in $W_2(O_2CAr)_4$ spectra, but rather, *both* are "masked" by the MLCT transitions. In $W_2R_2(O_2CAr)_4$ species, where the MLCT bands are blue-shifted, the triplet $\delta \rightarrow \delta^*$ transition is all that is observable. This suggests that Cotton's second argument is more pertinent, i.e., that the doublet nature of the intense band *is* specific to the arene-carboxylate compounds where conjugation between phenyl and carboxylate π and π^* systems can occur. This would explain why in the compound $W_2(O_2CC_6H_2[2,4,6\text{-Me}_3])_4$, where the substituted phenyl rings are kept nearly perpendicular to the planes of the carboxylate groups, only a single MLCT transition is observed along with the triplet $\delta \rightarrow \delta^*$ transition at lower energy.[41]

We have chosen to examine the extent of interaction between the carboxylate and arene π and π^* systems in the model compound $C_6H_5CO_2^-$ with the aid of the Fenske-Hall calculational method.[81]

A correlation diagram for $C_6H_5CO_2^-$ which shows occupied π orbitals only is shown in Figure 23. Transformation of the results into the canonical orbitals of CO_2^{2-} and $C_6H_5^+$ was performed, which allows for the assessment of the bonding picture in terms of the molecular orbitals of the two fragments. The interaction of a π ($2b_1$) orbital (C_{2v} symmetry) of the $C_6H_5^+$ fragment with the CO_2^{2-} π ($1b_1$) orbital produces the in-phase and out-of-phase combinations of π orbitals ($2b_1$ and $3b_1$, respectively) of $C_6H_5CO_2^-$. The $2b_1$ orbital has a greater amount of carboxylate character than ring character and vise versa. The $2a_2$ orbital of $C_6H_5CO_2^-$ is the unperturbed $1a_2$ lone-pair orbital of CO_2^{2-}. The same type of interaction is found for the unoccupied π^* orbitals of $C_6H_5^+$ and CO_2^{2-}, which demonstrates that arene and carboxylate π and π^* orbitals do interact. The point of this exercise is that a set of four carboxylate π^* orbitals of individual carboxylate groups will form symmetry-adapted linear combinations of a_{2g}, b_{2g}, and e_u symmetry in the D_{4h} point group. The δ orbital has b_{2g} symmetry and hence a $b_{2g} \rightarrow e_u$ charge-transfer transition is allowed by symmetry and has been assigned to the single intense MLCT transition in the alkyl-carboxylate complexes. When the carboxylate π^* orbital (b_1 under C_{2v} symmetry) is allowed to interact with a $C_6H_5^+$ fragment, we see that the interaction produces *two* b_1 combinations (C_{2v} symmetry) of π^* orbitals. Now, a set of four $C_6H_5CO_2^-$ ligands will form symmetry-adapted linear combinations of $2a_{2g}$, $2b_{2g}$, and $2e_u$ in the D_{4h} point group. Thus under D_{4h} symmetry there will be *two* allowed $b_{2g} \rightarrow e_u$ MLCT transitions. Furthermore, the filled carboxylate π, arene π, and M–M

(77) San Filippo, J.; Sniadoch, H. J. *Inorg. Chem.* **1976**, *15*, 2209.

(78) We observe a similar spectrum for $W_2(np)_2(O_2CC_6H_2[2,4,6\text{-Me}_3])_4$. See Table XII.

(79) Molar absorptivity coefficients were not reported in ref 41.

(80) Extinction coefficients were measured from the base line. True extinction coefficients associated with bands that appear as shoulders, e.g., the $^3(\delta \rightarrow \delta^*)$ ($^1A_{1g} \rightarrow {}^3A_{2u}$) transition in $W_2(np)_2(O_2CPh)_4$ in Figure 22, are probably significantly smaller.

(81) Hall, M. B.; Fenske, R. F. *Inorg. Chem.* **1972**, *11*, 768.

Table XIII. Calculated and Experimental Electronic Absorption Spectra for $W_2(O_2CR')_4$ and $W_2(O_2CR')_4R_2$ Molecules[a]

| compd | transition | excited states[b] | type[c] | ν, cm^{-1} (10^4) | | ϵ, M^{-1} cm^{-1} |
				calcd[d]	obsd	
D_{4h}-$W_2(O_2CEt)_4$	$2b_{2g} \rightarrow 2b_{1u}$	$^3A_{2u}$	$^3(\delta \rightarrow \delta^*)$		1.13	6.3×10^1
	$2b_{2g} \rightarrow 2b_{1u}$	$^1A_{2u}$	$^1(\delta \rightarrow \delta^*)$	1.25		
	$2b_{2g} \rightarrow 7e_u$	^1E_u	$\delta \rightarrow \pi^*_{(oco)}$	(3.56)	2.79	1.3×10^4
	$6e_u \rightarrow 5e_g$	$^1A_{2u}$	$\pi \rightarrow \pi^*$	3.54	4.07	2.9×10^3
C_{2h}-$W_2(O_2CEt)_4(np)_2$	$8b_g \rightarrow 10a_u$	^3B_u	$^3(\delta \rightarrow \delta^*)$		1.66	3.0×10^1
	$8b_g \rightarrow 10a_u$	^1B_u	$^1(\delta \rightarrow \delta^*)$	1.28	2.17	6.0×10^2
	$8b_g \rightarrow 11a_u, 16b_u$	$^1B_u, {}^1A_u$	$\delta \rightarrow \pi^*_{(oco)}$	3.42	2.93	1.8×10^4
	$15b_u \rightarrow 16a_g$	^1B_u	$\sigma_{(wc)} \rightarrow \sigma^*_{(wc)}$	2.43	3.41	4.5×10^4
	$14b_u \rightarrow 9b_g$	^1A_u	$\pi \rightarrow \pi^*$	3.68	3.89	1.3×10^4
	$14b_u \rightarrow 17a_g$	^1B_u	$\pi \rightarrow \pi^*$	3.79	3.97	1.1×10^4
	$9a_u \rightarrow 9b_g$	^1B_u	$\pi \rightarrow \pi^*$	3.88	4.07	1.0×10^4
	$9a_u \rightarrow 17a_g$	^1A_u	$\pi \rightarrow \pi^*$	3.99	4.17	9.3×10^3

[a] Calculated values are for the model compounds $W_2(O_2CH)_4$ and $W_2(O_2CH)_4(CH_3)_2$. The value in parentheses is estimated based on nearby calculated transition states and should be accurate to ca. 0.1 eV. [b] The ground states are $^1A_{1g}$ and ^1A_g for D_{4h} and C_{2h} point groups, respectively. Allowed transitions are to excited states of A_{2u} or E_u in D_{4h} symmetry and A_u or B_u in C_{2h} symmetry. [c] π, π^*, δ, and δ^* denote the W–W character of mainly metal orbitals. $\pi^*_{(oco)}$ denotes a carboxylate π-antibonding orbital and $\sigma_{(wc)}$ and $\sigma^*_{(wc)}$ denote W–C σ-bonding and -antibonding orbitals, respectively. [d] Band positions were obtained from the calculated values using the relationship 1 eV = 8065.5 cm^{-1}. Values calculated via Slater's spin-unrestricted transition-state procedure, giving a simple average of singlet and triplet energies. Bagus, P. S.; Bennett, B. I. *Int. J. Quantum Chem.* **1975** *9*, 143.
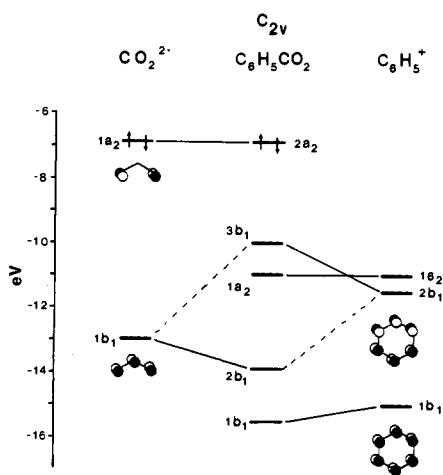

Figure 23. Correlation diagram for $C_6H_5CO_2^-$ showing only occupied π orbitals. This diagram shows a correlation of $C_6H_5CO_2^-$ π orbitals to those of the fragments $C_6H_5^+$ and CO_2^{2-} under C_{2v} symmetry. The HOMOs are denoted by the spin-pairing of arrows.

δ orbitals all have b_{2g} symmetry in D_{4h} and are expected to interact. We have placed these observations into a qualitative interaction diagram showing only the e_u (L π^*) and b_{2g} (M–M δ and L π) interactions under D_{4h} symmetry in Figure 24. Qualitatively this accounts for the presence of two intense ($\epsilon \sim 30\,000$ M^{-1} cm^{-1}) MLCT bands when the phenyl groups are coplanar with the CO_2 moiety in $M_2(O_2CAr)_4$ and $M_2R_2(O_2CAr)_4$ compounds.

The $\sigma_{(wc)}$ to $\sigma^*_{(wc)}$ Transition. The last absorption feature deserving comment is the most prominent band in the spectra of $W_2R_2(O_2CR')_4$ compounds. This extremely intense band ($\epsilon \sim 45\,000$ M^{-1} cm^{-1}) at ca. 34\,000 cm^{-1} present in $W_2R_2(O_2CR')_4$ spectra but absent in $W_2(O_2CR')_4$ spectra is tentatively assigned to the $\sigma_{(wc)} \rightarrow \sigma^*_{(wc)}$ ($^1A_g \rightarrow {}^1B_u$) dipole-allowed transition. This corresponds to the transition from the $15b_u$ (W–C σ) to $10a_g$ (W–C σ^*) orbitals of Figure 10.

Calculated Transition Energies. The relativistic Xα–SW transition energies for the model compounds $W_2(O_2CH)_4$ and $W_2(CH_3)_2(O_2CH)_4$ are listed in Table XIII and compared to experimental spectra. The values in the table were calculated via Slater's spin-unrestricted transition-state procedure giving a simple average of singlet and triplet energies.[82] It is clear that the
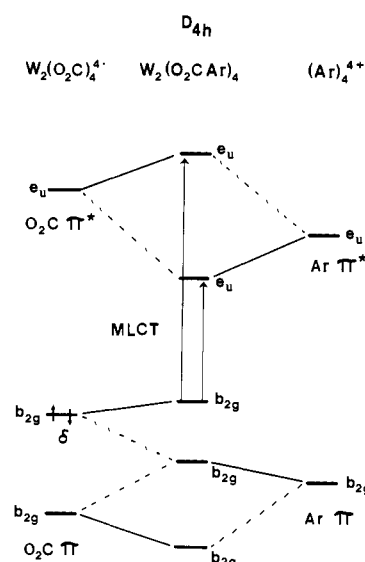

Figure 24. Schematic correlation diagram depicting the interaction between the arene π and π^* orbitals and the CO_2 π and π^* and M–M δ orbitals in $W_2(O_2CAr)_4$ compounds in D_{4h} symmetry. Only the relevant b_{2g} and e_u orbitals are shown.

calculated transitions are generally too low in energy, especially for the $\delta \rightarrow \delta^*$ transitions in which they appear to be a factor of 2 too small when compared to the proposed singlet transition of $W_2(np)_2(O_2CEt)_4$ (vide supra).

Despite the problems with the calculated transition energies, some valuable information regarding the experimental spectra can be extracted from them. Most importantly, the calculations predict that the $\delta \rightarrow \delta^*$ transitions should be the lowest energy transitions for both species. Secondly, the calculations suggest that the two species should show very similar spectra (as they do), and with the exception of $\delta \rightarrow \pi_{(oco)}^*$ MLCT transitions, the calculations suggest the correct order of transitions and have therefore been valuable toward our interpretation of the electronic spectra.

Concluding Remarks

The experimental data and the SCF–Xα–SW calculation[44] are in agreement with respect to the assignment of the valence M–M MO configuration as $\pi^4\delta^2$ in $W_2R_2(O_2CR')_4$ compounds. Formally these d^3–d^3 dinuclear compounds have M–M triple bonds ($\pi^4\delta^2$) lacking a σ component. As we have repeatedly pointed out, this is only a formalism since there are three MOs that have significant

(82) The transition-state formalism is described in: Slater, J. C. *Quantum Theory for Molecules and Solids. The Self-Consistent Field for Molecules and Solids*; McGraw-Hill: New York, 1974; Vol. 4.

M–M σ components, two being M–M bonding and one being M–M antibonding. It is, however, extremely unusual for a multiple bond between two elements to lack a formal σ bond. The diamagnetic diatomic molecule C_2 is the only homodiatomic molecule of the first period to contain a double bond formally lacking a σ component: $1\sigma^2 1\sigma^{*2} 2\sigma^2 2\sigma^{*2} 1\pi^4$.[83] The simple counting of electrons and cancellation of the σ and σ^* components leads to a double bond of configuration π^4 to first-order approximation. However, there is second-order 2s and 2p orbital mixing such that the $2\sigma^*$ becomes less antibonding and becomes an out-of-phase combination of lone-pair orbitals. The result is that the 2σ orbital remains the only orbital that is strongly σ bonding. Consequently C_2 has a shorter bond distance, 1.24 Å,[84] than that in ethylene, 1.34 Å, despite the fact that the valence MO descriptions of the double bonds approximate π^4 and $\sigma^2\pi^2$, respectively. The residual σ bonding in C_2 that results from second-order s–p mixing can be seen by an analysis of the Mulliken populations of the σ orbitals.[84,85]

It may be noted that for $W_2Bz_2(O_2C\text{-}t\text{-}Bu)_4$ and $W_2(np)_2$-$(O_2CEt)_4$, for which we obtained $^{13}C\{^1H\}$ spectra, we observe both a one-bond and a two-bond $^{183}W\text{-}^{13}C$ coupling: $^1J_{^{183}W\text{-}^{13}C} \sim 140$ Hz and $^2J_{^{183}W\text{-}^{13}C} \sim 14$ Hz. The two-bond W–C is almost certainly a reflection of W 6s–W 6s bonding. The ratio $^1J_{WC}/^2J_{WC}$ of 10 is similar to that for the $^{13}C\text{-}^{13}C$ couplings in propyne involving the methyl carbon, namely, $^1J_{CC} = 67.6$ Hz and $^2J_{CC} = 11.8$ Hz.[86]

In general there are always conceptual problems with σ orbitals in multiple bonds, even in simple diatomics. For example, carbon monoxide and dinitrogen have triple bonds ($\sigma^2\pi^4$) but for each there are in fact five occupied σ-type orbitals, some bonding, some antibonding, and some nonbonding (lone pair) in character. The full ramifications of the "σ-orbital problem" in the chemistry of dinuclear compounds having M–M bonds may be far-reaching.

There is the additional question of what factors favor the adoption of structure type I relative to II for compounds of formula $M_2R_2(O_2CX)_4$, and this matter is addressed in the following paper.[40]

Finally, aside from the interest in the electronic structure of the M–M multiple bond in $M_2R_2(O_2CR')_4$ compounds, it must be recognized that these compounds open new areas for synthesis. The photoinduced alkyl elimination reaction shown in eq 6 provides, for example, a simple route to $W_2(O_2CH)_4$, the hitherto unknown prototype of all $W_2(O_2CR')_4$ compounds.

Experimental Section

Physical Techniques. ^1H NMR spectra were recorded on a Nicolet NT-360 spectrometer at 360 MHz in dry and oxygen-free toluene-d_8, benzene-d_6, or methylene-d_2 chloride. ^{19}F NMR spectra were recorded on the same instrument at 340 MHz in benzene-d_6. All ^1H NMR chemical shifts are reported in ppm relative to the CHD_2 quintet of toluene-d_8 set at 2.09 ppm or the ^1H impurity in benzene-d_6 set at 7.15 ppm. ^{19}F NMR chemical shifts are reported in ppm relative to CF_3C-O_2H used as an external lock and set at –78.90 ppm relative to $CFCl_3$.

Infrared spectra were recorded on a Perkin-Elmer 283 spectrophotometer as Nujol mulls between CsI plates and referenced to polystyrene at 1601 cm^{-1}.

Electronic absorption spectra were recorded on a Perkin-Elmer 330 spectrophotometer. Samples were run vs. a solvent blank using matched 1.00-cm or 1.0-mm quartz cells. Extinction coefficients were measured from the base line. The true extinction coefficients associated with bands that appear as shoulders are probably significantly smaller. Extinction coefficients were reproducible to ±10%. Spectral grade solvents were used without further purification, except for degassing. A summary of electronic absorption data can be found in Table XII.

Electrochemical measurements were obtained with a PAR 173 po-

tentiostat and 175 programmer along with a Houston Instruments 2000 XY recorder. Cyclic voltammograms were referenced to a Ag/Ag$^+$ electrode. The working electrode was a platinum wire encased in a cobalt glass tipped electrode and polished smooth to provide an easily cleaned surface. The counter electrode was a platinum-gauze electrode. All CV's were carried out in a Vacuum Atmospheres drybox. A summary of electrochemical data can be found in Table X.

Elemental analyses were performed by Alfred Bernhardt Mikroanalytisches Laboratorium, Elbach, West Germany, and were handled with inert-atmosphere techniques. A summary of the analytical data can be found in Table I.

Photoelectron Spectral Measurements. The photoelectron spectra were obtained on a spectrometer featuring a 36-cm-radius hemispherical analyzer and other improvements described previously.[87]

Synthesis. All reactions were carried out under an atmosphere of dry and oxygen-free nitrogen using standard Schlenk and glovebox techniques. Carboxylic anhydrides and acids were purchased from Aldrich and were degassed via freeze–thaw cycles. Bisalkyltetrakis(dimethylamide)ditungsten and -dimolybdenum compounds were prepared by published procedures.[88] Acid-free anhydrides as well as anhydrous acids must be used to avoid decomposition.

$W_2Bz_2(O_2CEt)_4$. In a Schlenk reaction vessel $W_2Bz_2(NMe_2)_4$ (1.00 g, 1.38 mmol) was dissolved in toluene (20 mL). The flask was placed in an ice bath, and an excess (>4 equiv, 5.52 mmol) of propionic anhydride was added via syringe. The solution was stirred for several minutes and the color changed from yellow-brown to dark brown. The solvent was removed in vacuo to produce an oily solid. The solid was redissolved in a 1:1 hexane/toluene solution (ca. 20 mL) and filtered. The volume was reduced and the flask was cooled to –15 °C. After 2 days amber hexagonal plates were recovered by filtration (total yield 0.83 g, 72% based on tungsten).

^1H NMR (22 °C), benzene-d_6: major isomer, δ 3.65 (s, $^2J_{WH} = 13.4$ Hz, CH_2Ph), 2.77 (q, $^3J_{HH} = 7.6$ Hz, CH_2CH_3), 0.88 (t, $^3J_{HH} = 7.6$ Hz, CH_2CH_3); minor isomer, δ 3.84 (s, CH_2Ph), 2.33, 1.91 (q, $^3J_{HH} = 7.6$ Hz, CH_2CH_3), 1.13, 0.72 (t, $^3J_{HH} = 7.6$ Hz, CH_2CH_3).

IR (cm^{-1}): 320 (m), 427 (m), 438 (m), 535 (vw), 552 (w), 610 (m), 662 (w), 690 (s), 750 (s), 804 (m), 889 (ms), 995 (ms), 1024 (s), 1032 (s), 1077 (m), 1104 (w), 1148 (w), 1175 (w), 1210 (w), 1300 (vs), 1430 (vs), 1450 (vs), 1485 (vs), 1595 (m).

$W_2Bz_2(O_2CH)_4$. To a CH_2Cl_2 solution (10 mL) of $W_2Bz_2(O\text{-}i\text{-}Pr)_4$ (0.50 g, 0.69 mmol) at –78 °C was added 4 equiv of formic acid via a microliter syringe. The solution turned brown and was then warmed to room temperature. The solvent was removed in vacuo. A 1:1 hexane/toluene solution (ca. 20 mL) was used to extract the yellow compound. The solvent was removed to produce an oily solid, which was pure by ^1H NMR spectroscopy.

^1H NMR (22 °C), methylene-d_2 chloride: major isomer, δ 8.20 (s, $^3J_{WH} = 9.9$ Hz, O_2CH), 7.23 (d, ortho), 7.20 (t, meta), 6.98 (t, para), 3.25 (s, $^2J_{WH} = 14.1$ Hz, CH_2Ph); minor isomer, δ 8.80, 7.74 (s, O_2CH), 2.92 (s, CH_2Ph).

$W_2Bz_2(O_2CCMe_3)_4$. Four equivalents (5.52 mmol) of pivalic anhydride was added to a toluene solution (10 mL) of $W_2Bz_2(NMe_2)_4$ (1.0 g, 1.38 mmol) via a microliter syringe. The resulting dark brown solution was evaporated to dryness under dynamic vacuum to produce a viscous oil. Hexane (20 mL) was added and the volume was reduced. The flask was cooled to –78 °C for several days, after which amber plates had formed. The solution was removed via a cannula, and the crystals were dried in vacuo (total yield 0.32 g, 24%).

^1H NMR (22 °C), benzene-d_6: δ 3.48 (s, $^2J_{WH} = 14.1$ Hz, CH_2Ph), 1.12 (s, CMe_3), 7.40 (d, ortho), 7.21 (t, meta), 6.87 (t, para).

$^{13}C\{^1H\}$ (22 °C), benzene-d_6: δ 191.0 ($^2J_{WC} = 4.0$ Hz, O_2C), 73.85, ($^1J_{WC} = 122$ Hz and $^2J_{WC} = 13.6$ Hz, CH_2Ph).

IR (cm^{-1}): 445 (mw), 608 (m), 684 (m), 718 (w), 745 (m), 768 (w), 790 (mw), 795 (mw), 890 (m), 898 (mw), 1025 (m), 1032 (m), 1217 (s), 1361 (vs), 1411 (s), 1582 (br, s).

$W_2Bz_2(O_2CPh)_4$. Four equivalents (5.52 mmol) of benzoic anhydride was added to a toluene solution (10 mL) of $W_2Bz_2(NMe_2)_4$ (1.0 g, 1.38 mmol) via a solids addition tube. The solution turned purple. The solvent was evaporated to dryness after several minutes and a 1:1 hexane/toluene solution (10 mL) was added. The solution was filtered, giving an orange powder (0.61 g, 43% based on tungsten).

^1H NMR (22 °C), methylene-d_2 chloride: δ 3.60 (s, $^2J_{WH} = 13.7$ Hz,

(83) See, for example: (a) Gray, H. G.; Dekock, R. L. *Chemical Structure and Bonding*; W. A. Benjamin: Reading, MA, 1980; Chapter 4. (b) Albright, T. A.; Burdett, J. K.; Wangbo, M. *Orbital Interactions in Chemistry*; Wiley: New York, 1985; Chapter 6.

(84) Fougere, P. F.; Nesbett, R. K. *J. Chem. Phys.* 1966, 44, 285.

(85) Mulliken, R. S.; Ermler, W. C. *Diatomic Molecules, Results of ab Initio Calculations*; Academic: New York, 1977; Table 7, p 172.

(86) Weigert, F. J.; Roberts, J. D. *J. Am. Chem. Soc.* 1972, 94, 602.

(87) Hubbard, J. L.; Lichtenberger, D. L. *J. Am. Chem. Soc.* 1982, 104, 2132.

(88) (a) Chetcuti, M. J.; Chisholm, M. H.; Folting, K.; Haitko, D. A.; Huffman, J. C.; Janos, J. *J. Am. Chem. Soc.* 1983, 105, 1163. (b) Chisholm, M. H.; Haitko, D. A.; Huffman, J. C. *J. Am. Chem. Soc.* 1981, 103, 4046.

CH$_2$Ph), 7.84 (d, ortho O$_2$CPh), 7.38 (t, meta O$_2$CPh), 7.30 (t, para O$_2$CPh), 7.46 (d, ortho CH$_2$Ph), 7.32 (t, meta CH$_2$Ph), 7.05 (t, para CH$_2$Ph).

W$_2$Bz$_2$(O$_2$CMe)$_4$. In a Schlenk reaction vessel W$_2$Bz$_2$(NMe$_2$)$_4$ (0.50 g, 0.69 mmol) was dissolved in a minimal amount of CH$_2$Cl$_2$ (ca. 3 mL), and the flask was cooled to −78 °C. Slightly greater than 4 equiv (2.90 mmol) of acetic anydride in toluene was added over the course of 1 h via a dropping funnel. The solution turned from yellow-brown to an orange color. The solution was removed under vacuum to yield orange microcrystals (0.49 g, 91% based on tungsten).

^{1}H NMR (22 °C), benzene-d_6: major isomer, δ 7.50 (d, ortho), 7.27 (t, meta), 6.91 (t, para), 3.66 (s, $^2J_{WH}$ = 13.6 Hz, CH$_2$Ph), 2.34 (s, O$_2$CMe); minor isomer, 3.84 (s, CH$_2$Ph), 1.95, 1.45 (s, O$_2$CMe).

IR (cm^{-1}): 335 (ms), 423 (mw), 432 (mw), 551 (w), 600 (vw), 629 (m), 668 (s), 690 (ms), 698 (ms), 750 (ms), 755 (ms), 800 (m, br), 891 (mw), 906 (w), 933 (w), 995 (m), 1022 (s), 1031 (s), 1050 (s), 1088 (w, br), 1212 (w), 1260 (m), 1350 (s), 1425 (vs), 1453 (vs), 1488 (s), 1591 (ms).

W$_2$(np)$_2$(O$_2$CEt)$_4$. Greater than 4 equiv of propionic anhydride was added to a toluene solution (10 mL) of W$_2$(np)$_2$(NMe$_2$)$_4$ (1.0 g, 1.46 mmol) at 0 °C. The solution turned green, and after several minutes the solvent was removed in vacuo to produce bright green needles (1.02 g, 87% based on tungsten). Large crystals can be grown from hexane or CH$_2$Cl$_2$, and the compound can be sublimed at 120 °C under high vacuum onto a water-cooled probe.

^{1}H NMR (22 °C), benzene-d_6: δ 2.83 (q, $^3J_{HH}$ = 7.6 Hz, CH$_2$CH$_3$), 2.70 (s, $^2J_{WH}$ = 17.0 Hz, CH$_2$CMe$_3$), 1.46 (s, CH$_2$CMe$_3$), 0.99 (t, $^3J_{HH}$ = 7.6 Hz, CH$_2$CH$_3$).

^{13}C{^{1}H} NMR (22 °C), toluene-d_8: δ 186.0 (O$_2$C), 91.05 (CH$_2$CMe$_3$, $^1J_{WC}$ = 140.7 Hz, $^2J_{WC}$ = 14.9 Hz), 35.87 (C(CH$_3$)$_3$), 33.13 (C(CH$_3$)$_3$), 28.97 (CH$_2$CH$_3$), 11.79 (CH$_2$CH$_3$).

IR (cm^{-1}): 310 (m), 319 (m), 432 (m), 610 (m), 665 (w), 719 (w), 740 (w), 800 (m), 889 (ms), 1082 (s), 1093 (vs), 1105 (mw), 1135 (ms), 1199 (vs), 1358 (m), 1429 (m), 1482 (m).

Mass spectral data, m/z (%): 802 (11), 729 (<1), 674 (8), 660 (100), 548 (6.1).

W$_2$(np)$_2$(O$_2$CMe)$_4$. Greater than 4 equiv (5.84 mmol) of acetic anhydride was added to a toluene solution (10 mL) of W$_2$(np)$_2$(NMe$_2$)$_4$ (1.0 g, 1.46 mmol). After a few moments the solvent was removed in vacuo, yielding green microneedles (0.99 g, 91% based on tungsten). Recrystallization from toluene produced green hexagonal plates. It is also possible to sublime this compound at 120 °C under high vacuum. This compound is air-stable in the solid state.

^{1}H NMR (22 °C), benzene-d_6: δ 2.73 (s, $^2J_{WH}$ = 10.1 Hz, CH$_2$CMe$_3$), 2.45 (s, O$_2$CCH$_3$), 1.49 (s, CH$_2$CMe$_3$).

IR (cm^{-1}): 335 (s), 378 (w), 454 (w), 560 (vw), 598 (w), 631 (m), 669 (vs), 747 (w), 911 (m), 937 (m), 1011 (m), 1020 (m), 1042 (ms), 1090 (vs), 1107 (m), 1140 (s), 1348 (s), 1352 (s), 1359 (s), 1362 (s), 1411 (vs), 1435 (br, vs), 1492 (s).

W$_2$(np)$_2$(O$_2$CCF$_3$)$_4$. To a toluene solution (10 mL) of W$_2$(np)$_2$-(NMe$_2$)$_4$ (1.0 g, 1.46 mmol) was added 4 equiv of trifluoroacetic anhydride. The solution turned dark red and the solvent was removed in vacuo, giving red needles (1.15 g, 82% based on tungsten). This compound can be recrystallized from hexane and can also be sublimed. An alternate synthesis involves addition of an excess of trifluoroacetic acid to a toluene solution of W$_2$(np)$_2$(O$_2$CMe)$_4$, with standard workup.

^{1}H NMR (22 °C), benzene-d_6: 2.65 (s, $^2J_{WH}$ = 7.9 Hz, CH$_2$CMe$_3$), 1.07 (s, CH$_2$CMe$_3$).

^{19}F NMR (22 °C), benzene-d_6: δ −72.73 (s, CF$_3$).

IR (cm^{-1}): 340 (mw), 394 (mw), 500 (ms), 535 (ms), 651 (mw), 668 (m), 738 (vs), 765 (m), 772 (s), 868 (vs), 908 (m), 933 (mw), 1100 (vs, br), 1150–1270 (vs), 1361 (m), 1370 (ms), 1445 (s), 1500 (w), 1525 (mw), 1558 (s), 1570 (s), 1576 (s).

Mass spectral data, m/z (%): 961.5 (12), 942.5 (4.4), 819.4 (52), 800.4 (27).

In an NMR tube W$_2$(np)$_6$ was reacted with trifluoroacetic acid, producing a dark yellow-orange solution within seconds of adding the acid. The ^{1}H NMR spectrum was identical with that of W$_2$(np)$_2$(O$_2$CCF$_3$)$_4$ along with neopentane (0.87 ppm). The ^{19}F spectrum suggested that both W$_2$(np)$_2$(O$_2$CCF$_3$)$_4$ and W$_2$(np)$_2$(O$_2$CCF$_3$)$_4$ were produced in the reaction in approximately a 3:1 ratio.

W$_2$(np)$_2$(O$_2$CCMe$_3$)$_4$. To a methylene chloride solution (10 mL) of W$_2$(np)$_2$(NMe$_2$)$_4$ (0.50 g, 0.73 mmol) was added slightly greater than 4 equiv of pivalic anhydride. The solution was stirred for 1 h and then the solvent was removed in vacuo to give an oily green solid. Hexane (20 mL) was used to extract the green compound, and the resultant solution was filtered through a fine frit. The solvent was removed in vacuo to give a green microcrystalline solid in 80% yield based on tungsten.

^{1}H NMR (22 °C), benzene-d_6: δ 2.60 (s, $^2J_{WH}$ = 9.9 Hz, CH$_2$CMe$_3$,

1.43 (s, CH$_2$CMe$_3$), 1.26 (s, O$_2$CCMe$_3$).

W$_2$(np)$_2$(O$_2$CH)$_4$. To a toluene solution (10 mL) of W$_2$(np)$_2$-(O$_2$CMe)$_4$ (0.5 g, 0.73 mmol) an excess (>4 equiv) of formic acid was added. The solution was stirred for 24 h. The green microcrystalline precipitate was extracted with a 1:1 hexane/toluene solution (30 mL). The solvent was removed in vacuo to give the title compound (0.48 g, 95% yield). This compound was recrystallized from toluene (ca. 6 mL) by adding a minimal amount of solvent and then heating in a hot water bath until all of the solid dissolved. The flask was then allowed to cool to room temperature. This produced large green cubes. It was very difficult to obtain totally pure material by this method, with small amounts of W$_2$(np)$_2$(O$_2$CH)$_3$(O$_2$CMe) usually being present based on ^{1}H NMR.

An alternate synthesis involves adding an excess of formic acid to a toluene solution (10 mL) of W$_2$(np)$_2$(O-i-Pr)$_4$ (0.50 g, 0.67 mmol). The solution was stirred for 30 min and then the solvent removed in vacuo. This method provides pure compound free of other products in near-quantitative yields.

^{1}H NMR (22 °C), benzene-d_6: δ 2.65 (s, $^2J_{WH}$ = 9.6 Hz, CH$_2$CMe$_3$), 1.36 (s, CH$_2$CMe$_3$), 7.55 (s, $^3J_{WH}$ = 9.7 Hz, O$_2$CH).

IR (cm^{-1}): 378 (s), 467 (s), 498 (ms), 680 (w), 720 (w), 747 (w), 773 (vs), 909 (mw), 931 (mw), 979 (mw), 1090 (vs), 1202 (m), 1238 (ms), 1305 (s), 1336 (s), 1355 (w), 1362 (m), 1376 (m), 1465 (s), 1502 (s), 1945 (mw, br).

Mass spectral data, m/z (%): 690 (4.5), 619 (1.3), 562 (<1), 548 (19), 504 (<1).

W$_2$(np)$_2$(O$_2$CMe)$_2$(O$_2$CCF$_3$)$_2$. In a Schlenk flask W$_2$(np)$_2$(O$_2$CMe)$_4$ (1.0 g, 1.46 mmol) was dissolved in toluene (10 mL). Two equivalents (2.92 mmol) of trifluoroacetic acid in toluene (10 mL) was added via a dropping funnel to the solution at 0 °C over a period of 1 h. The color changed from green to yellow-orange. The solution was stirred for 2 days, after which the solvent was removed in vacuo. The solid was recrystallized from hexane (0.89 g, 72%). Small amounts of other products such as W$_2$(np)$_2$(O$_2$CMe)$_x$(O$_2$CCF$_3$)$_y$ (x = 3, y = 1; x = 1, y = 3) can be seen in both the ^{1}H and ^{19}F NMR spectra.

^{1}H NMR (22 °C), benzene-d_6: δ 2.72 (s, $^2J_{WH}$ = 9.0 Hz, CH$_2$CMe$_3$), 2.13 (s, O$_2$CMe), 1.29 (s, CH$_2$CMe$_3$).

^{19}F NMR (22 °C), benzene-d_6: δ −72.26 (s, CF$_3$).

W$_2$(np)$_2$(O$_2$CPh)$_4$. Four equivalents of (PhCO)$_2$O (1.32 g, 5.84 mmol) was added to a toluene solution (10 mL) of W$_2$(np)$_2$(NMe$_2$)$_4$ (1.0 g, 1.46 mmol) via a solids addition tube. (For this reaction it was important *not* to add an excess of anhydride, because it was not easy to separate the anhydride from the mixture of products.) The toluene was removed in vacuo and a 1:1 hexane/toluene solution (10 mL) was used to wash the solid. This removed most of the (PhCO)NMe$_2$ byproduct. The red-green microcrystals were recrystallized from toluene (0.71 g, 49%). The crystals appear to be dichroic, with red and green faces.

^{1}H NMR (22 °C), benzene-d_6: δ 8.13 (d, ortho), 6.94 (t, meta), 6.79 (t, para), 3.26 (s, $^2J_{WH}$ < 6 Hz, CH$_2$CMe$_3$), 1.75 (s, CH$_2$CMe$_3$).

IR (cm^{-1}): 404 (m), 447 (w), 482 (m), 663 (w), 682 (s), 709 (s), 712 (s), 850 (m), 908 (vw), 931 (m), 1029 (m), 1070 (m), 1090 (s), 1155 (vw), 1162 (vw), 1181 (vw), 1202 (w), 1232 (m), 1359 (m), 1378 (s), 1433 (m), 1483 (m).

Mass spectral data, m/z (%): 994 (<1), 852 (3.2).

W$_2$(np)$_2$(O$_2$CC$_6$H$_4$-p-OMe)$_4$. Four equivalents (1.67 g, 5.84 mmol) of p-methoxybenzoic anhydride was added to a toluene solution (10 mL) of W$_2$(np)$_2$(NMe$_2$)$_4$ (1.0 g, 1.46 mmol) via a solids addition tube. The solution immediately turned purple, and green-red needles began to precipitate. The toluene was removed in vacuo and the resulting solid was washed several times (3 × 5 mL) with a 2:1 hexane/toluene solution. The product was then recrystallized from toluene (1.13 g, 70%).

^{1}H NMR (22 °C), benzene-d_6: δ 8.13 (d, ortho), 6.52 (d, meta), 3.29 (s, $^2J_{WH}$ = 9.7 Hz, CH$_2$CMe$_3$), 3.06 (s, OMe), 1.85 (s, CH$_2$CMe$_3$).

IR (cm^{-1}): 401 (w), 438 (w), 518 (w), 566 (vvw), 625 (s), 637 (ms), 698 (mw), 771 (s), 845 (s), 859 (m), 1031 (s), 1088 (s), 1094 (s), 1107 (mw), 1172 (vs), 1239 (m), 1260 (vs), 1300 (mw), 1312 (m), 1400 (vs), 1516 (s), 1583 (m), 1608 (vs).

W$_2$(np)$_2$(O$_2$CCHPh$_2$)$_4$. To a toluene solution (10 mL) of W$_2$(np)$_2$-(O$_2$CMe)$_4$ (0.6 g, 0.81 mmol) was added 4 equiv (0.69 g, 3.24 mmol) of Ph$_2$CHCO$_2$H via a solids addition tube. The solution turned from green to yellow almost immediately. The solvent was removed in vacuo after 30 min of stirring. Hexane (20 mL) was used to extract the yellow powder and the solution was filtered. The solvent was removed under vacuum to give the title compound (0.80 g, 73%).

^{1}H NMR (22 °C), benzene-d_6: δ 5.48 (s, CHPh$_2$), 2.09 (s, $^2J_{WH}$ = 9.5 Hz, CH$_2$CMe$_3$), 0.77 (s, CH$_2$CMe$_3$).

W$_2$(np)$_2$(O$_2$CC$_6$H$_2$[2,4,6-Me$_3$])$_4$. To a toluene solution (10 mL) of W$_2$(np)$_2$(OCHMe$_2$)$_4$ (0.30 g, 0.40 mmol) was added 4 equiv of mesitylbenzoic acid (0.26 g, 1.6 mmol). The yellow solution was stirred for

1 h, after which the solvent was removed in vacuo. A 1:1 mixture of hexane/toluene (5 mL) was used to wash the yellow solid, after which it was dried for 30 min under high vacuum. The yield was 0.35 g (75%) of a yellow powder.

^{1}H NMR (22 °C), benzene-d_6: δ 6.66 (s, $C_6H_2Me_3$), 3.06 (s, $^2J_{WH}$ = 9.4 Hz, CH_2CMe_3), 2.45 (s, o-Me), 2.05 (s, p-Me), 1.47 (s, CH_2CMe_3).

Reaction of $W_2Me_2(NMe_2)_4$ with $(MeCO)_2O$. In a Schlenk flask $W_2Me_2(NMe_2)_4$ (0.30 g, 0.52 mmol) was dissolved in CH_2Cl_2 (3 mL), and the flask was cooled to −78 °C. Slightly greater than 4 equiv of acetic anhydride was added to the solution via a syringe. The solution was mixed and after a few minutes a light brown precipitate began to form. After 1 h the solvent was removed via a cannula, and the solid was dried in vacuo for 1 h. The yield of $W_2Me_2(O_2CMe)_4$ was 0.15 g, 45%.

^{1}H NMR (22 °C), benzene-d_6: δ 3.03 (s, Me), 3.00, 2.14 (s, O_2CMe).

Reaction of $W_2Me_2(NMe_2)_4$ with $(PhCO)_2O$. $W_2Me_2(NMe_2)_4$ (0.30 g, 0.52 mmol) was placed in a Schlenk flask and a minimum amount of CH_2Cl_2 (3 mL) was added to dissolve the solid. The flask was then cooled to −78 °C and 4 equiv of benzoic anhydride in toluene (5 mL) was added by using a pressure-equalized dropping funnel over a period of 1 h. At the end of this period the solution had turned purple and an orange precipitate had formed. The solid was filtered and washed with an 1:2 CH_2Cl_2/hexane solution (5 mL). A 64% yield of $W_2Me_2(O_2CPh)_4$ was isolated as an orange powder, which was sparingly soluble in CH_2Cl_2 or toluene.

^{1}H NMR (22 °C), benzene-d_6: δ 7.97 (d, ortho), 6.89 (t, meta), 6.80 (t, para), 2.37 (s, CH_3, $^2J_{WH}$ = 9.0 Hz).

IR (cm^{-1}): 487 (mw), 512 (m), 648 (w), 678 (m), 690 (m), 719 (s), 800 (mw), 850 (m), 932 (w), 943 (w), 1023 (m), 1072 (w), 1121 (s), 1134 (w), 1153 (w), 1260 (mw), 1289 (w), 1308 (vw), 1394 (s), 1431 (m), 1471 (vs).

$W_2(CH_2SiMe_3)_2(O_2CMe)_4$. To a toluene solution (10 mL) of W_2-$(CH_2SiMe_3)_2(NMe_2)_4$ (0.50 g, 0.70 mmol) at 0 °C was added an excess of acetic anhydride. The solution was stirred for 30 min, after which the solvent was evaporated in vacuo. The green compound was extracted with hexane (10 mL), and the solution was filtered. The solvent was removed from the filtrate in vacuo to give a 50% yield of the title compound.

^{1}H NMR (22 °C), benzene-d_6: δ 2.40 (s, O_2CMe), 1.97 (s, $^2J_{WH}$ = 12.6 Hz, CH_2SiMe_3), 0.42 (s, CH_2SiMe_3).

IR (cm^{-1}): 338 (ms), 490 (mw), 580 (mw), 609 (w), 629 (m), 668 (ms), 702 (ms), 742 (m), 752 (m), 838 (s), 912 (m), 938 (w), 960 (mw), 1040 (mw), 1240 (ms), 1250 (m), 1329 (mw), 1350 (ms), 1440 (vs).

$W_2(CH_2CHMe_2)_2(O_2CMe)_4$. An excess of acetic anhydride was added to a CH_2Cl_2 solution (10 mL) of $W_2(CH_2CHMe_2)_2(NMe_2)_4$ (0.35 g, 0.53 mmol) at −78 °C. The solution was warmed to room temperature and the solvent was removed in vacuo. Using a water-cooled cold finger the yellow compound was sublimed at 100–120 °C under high vacuum to give a 55% yield.

^{1}H NMR (22 °C), benzene-d_6: δ 3.32 (multiplet, J = 6.5 Hz, $CHMe_2$), 2.56 (d, J = 6.5 Hz, $^2J_{WH}$ = 10.4 Hz, CH_2CHMe_2), 2.45 (s, Me), 1.35 (d, $CHMe_2$, J = 6.5 Hz).

$W_2(CH_2CHMe_2)_2(O_2CPh)_4$. Four equivalents of benzoic anhydride (0.70 g, 3.1 mmol) was added to a CH_2Cl_2 solution (10 mL) of W_2-$(CH_2CHMe_2)_2(NMe_2)_4$ (0.5 g, 0.76 mmol) at −78 °C. The solution was warmed to room temperature and the solvent removed in vacuo. A 2:1 mixture of hexane/toluene (10 mL) was used to extract the orange compound and the solution was filtered. The filtrate was reduced to about 1 mL and placed in the freezer. After 24 h at −20 °C dark green-red needles had formed in ca. 30% yield.

^{1}H NMR (22 °C), benzene-d_6: δ 8.08 (d, ortho), 6.92 (t, meta), 6.79 (t, para), 3.66 (multiplet, $CHMe_2$), 3.06 (d, CH_2CHMe_2), 1.59 (d, $CHMe_2$).

$W_2(o\text{-}MeC_6H_4)_2(O_2CEt)_4$. A toluene solution (5 mL) of $W_2(o\text{-}MeC_6H_4)_2(NMe_2)_4$ (0.30 g, 0.41 mmol) was cooled to −78 °C whereupon 4 equiv of propionic anhydride was added via a microsyringe. The solution was agitated and after a few minutes a light yellow precipitate had formed. The solution was removed with a cannula and the solids were dried in vacuo. The yield of yellow powder was 25%.

^{1}H NMR (22 °C), benzene-d_6: major isomer, δ 8.85, 7.32, 7.25, 2.99 (s, Me), 2.82 (q), 0.93 (t); minor isomer, δ 9.72, 2.32 (q), 2.15 (q), 1.62 (s), 1.54 (s), 1.06 (t), 0.98 (t), 0.80 (t).

$W_2(p\text{-}MeC_6H_4)_2(O_2CEt)_4$. A similar procedure of that of the o-tolyl complex was used and produced a 30% yield of a yellow powder.

^{1}H NMR (22 °C), benzene-d_6: major isomer, δ 8.82, 7.26, 2.84 (q), 2.09 (s, Me), 0.96 (t); minor isomer, δ 8.10, 7.40, 2.38, 2.17, 2.27, 1.06, 0.91.

$Mo_2(np)_2(O_2CMe)_4$. A CH_2Cl_2 solution (10 mL) of $Mo_2(np)_2$-

$(NMe_2)_4$ (0.50 g, 0.98 mmol) was cooled to −78 °C and 4 equiv of acetic anhydride was added. The solution immediately turned yellow. The solution was warmed to room temperature and the solvent was removed in vacuo, leaving a yellow-orange powder. The powder was recrystallized from toluene to give orange crystals in 60% yield. Some $Mo_2(O_2CMe)_4$ is also produced.

^{1}H NMR (22 °C), benzene-d_6: δ 2.78 (s, CH_2CMe_3), 2.14 (s, O_2CMe), 1.38 (s, CH_2CMe_3).

IR (cm^{-1}): 240 (vs), 278 (m), 335 (mw), 368 (ms), 628 (mw), 658 (mw), 672 (s), 910 (w), 932 (w), 1002 (mw), 1019 (w), 1045 (m), 1070 (vs), 1196 (mw), 1239 (m), 1342 (m), 1349 (m), 1353 (m), 1360 (m), 1371 (m), 1410 (ms), 1443 (vs), 1490 (m), 1500 (m), 1510 (ms).

$W_2(O_2CR)_4$ (R = Et, CF$_3$, Ph, p-PhOMe). These compounds were all prepared by adding the appropriate acid anhydride to toluene solutions of $W_2Et_2(NMe_2)_4$ at 25 °C.[33,86] The solvent was removed in vacuo and the compounds were purified by sublimation. The purity of the compounds was checked by ^{1}H NMR. These compounds were prepared in this manner in order to avoid the presence of axially coordinated solvent.

$W_2(O_2CH)_4$. After photolysis of a benzene/cyclohexadiene (10:1) solution of either $W_2(np)_2(O_2CH)_4$ or $W_2Bz_2(O_2CH)_4$ with a Hanovia water-cooled, low-pressure Hg lamp, $W_2(O_2CH)_4$ can be recovered as yellow-green needles in 60 and 80% yields, respectively. $W_2(O_2CH)_4$ is insoluble in the common deuterated solvents and this precluded any NMR spectrometric analyses. The molecule was characterized by mass spectrometry and gave a molecular ion m/z (%) of 548 (0.7), whose isotopic distribution was similar to that calculated for $W_2(O_2CH)_4$.

Crystallographic Studies. General operating procedures and listings of programs have been previously published.[89] Crystal data for $W_2Bz_2(O_2CEt)_4$, $W_2(np)_2(O_2CEt)_4$, $W_2(np)_2(O_2CPh)_4$, $W_2(np)_2$-$(O_2CH)_4$, and $W_2(np)_2(O_2CMe)_2(O_2CCF_3)_2$ are given in Table VIII. Suitable crystals were transferred to the goniostat by using standard inert-atmosphere handling techniques employed by the IUMSC and cooled with a gas flow cooling system.

$W_2Bz_2(O_2CEt)_4$. A systematic search of a limited hemisphere of reciprocal space revealed a set of diffraction maxima that could be indexed as monoclinic, space group $P2_1/c$.

Data were collected by using a standard moving crystal–moving detector technique, and the structure was solved by a combination of direct methods, Fourier techniques, and Patterson synthesis. All atoms, including hydrogen atoms, were located and refined. In general, the hydrogen atoms are well-behaved, although one of the benzyl hydrogen distances is shorter than normal. The molecule lies on a center of inversion in the crystal lattice. A final difference Fourier is featureless; the three largest peaks (1.1–1.8 e/Å^3) lie within 1.0 Å of the tungsten position.

ψ scans of several reflections indicated error due to absorption was less than 5%, and due to the irregular nature of the faces on the crystal, no attempt was made to perform the correction. The packing efficiency was checked by using the AVOID program, the results of which are available in the full structure report.

$W_2(np)_2(O_2CEt)_4$. After the sample was mounted and cooled in the usual manner, a reciprocal lattice search revealed no systematic absences, an indication of a triclinic space group. Statistical tests and subsequent solution and refinement of the structure confirmed the centrosymmetric space group $P\bar{1}$ to be the correct choice.

The structure was solved by first locating the tungsten atoms from a Patterson synthesis, and subsequent Fourier synthesis. ψ scans of several reflections varied significantly and an analytical absorption correction was applied. A difference Fourier phased on the non-hydrogen parameters located approximately half of the hydrogen positions. Due to their poor resolution in the difference synthesis, all hydrogens were included in the final cycles in fixed, idealized positions. A final difference Fourier revealed no peaks larger than 0.45 e/Å^3, except for several near the tungsten atoms.

$W_2(np)_2(O_2CPh)_4$. A suitable sample was cleaved from a larger crystal and transferred to the goniostat, where it was cooled to −157 °C for characterization and data collection. A systematic search of a limited hemisphere of reciprocal space revealed a set of diffraction maxima that could be indexed as monoclinic, space group $P2_1/c$. Subsequent solution and refinements confirmed the choice.

The structure was solved by a combination of direct methods (MULTAN 78) and Fourier techniques and refined by full-matrix least squares. All hydrogen atoms were located and refined. A final difference Fourier was featureless, the largest peak being 0.81 e/Å^3.

(89) Chisholm, M. H.; Folting, K.; Huffman, J. C.; Kirkpatrick, C. C. *Inorg. Chem.* **1984**, *23*, 1021.

W₂(np)₂(O₂CH)₄. Several crystals were examined at −158 °C and found to have large uneven mosiac character and, in general, were split along one axis. It was then noticed that the crystals appeared to fracture slightly upon entering the cold stream. The temperature control system was adjusted to give a temperature of −50 °C, and several other crystals were examined. By adjusting the temperature, it was determined that a gradual phase transition appears to occur beginning at (or near) −60 °C. When crystals are cooled, the well-defined peaks begin to broaden and eventually split.

A systematic search of a limited hemisphere of reciprocal space located a set of diffraction maxima of tetragonal symmetry with extinctions coresponding to the space group $I4_1/a$. Subsequent solution and refinement confirmed this choice.

The structure was solved by direct methods (MULTAN 78) and Fourier techniques and refined by full-matrix least squares. Only a few of the hydrogen atoms appeared to be present in a difference Fourier phased on the non-hydrogen parameters. For this reason the final cycles contained the hydrogens in fixed idealized positions. Interestingly enough, the hydrogens that could be located were the formate protons, and not the neopentyl protons.

The large thermal parameters of the structure probably reflect the instability of the crystal near the phase transition. No attempt was made to carefully characterize the phase transition other than to note that the lower temperature phase appears to be orthorhombic, with a ca. 0.2 Å longer than b. The splitting observed is thus more of an indication of a "twin" than a split crystal. A final difference Fourier was featureless, other than two peaks of 1.8 and 1.6 e/Å³ located 0.5 Å from the metal atom. All other peaks were less than 0.8 e/Å³.

W₂(np)₂(O₂CMe)₂(O₂CCF₃)₂. One of the larger crystals was cleaved to form a nearly equidimensional rectangular fragment with well-formed faces. After the sample was transferred to the goniostat, it was cooled to −158 °C. A systematic search revealed absences corresponding to the unique space group $P2_1/n$. Subsequent solution and refinement of the structure confirmed this choice. The structure was solved by direct methods (MULTAN 78) and Fourier techniques and refined by full-matrix least squares. A ψ scan indicated a significant absorption problem, so a correction was applied. A difference Fourier phased on non-hydrogen atoms located approximately half of the hydrogen positions, and for the final cycles all hydrogen atoms were placed in idealized fixed positions.

The poorly shaped thermal ellipsoids on several of the atoms are probably best described as artifacts of the absorption correction, although the six fluorine atoms all appear to have physically significant amplitudes.

Mo₂(np)₂(O₂CMe)₄. A systematic search of a limited hemisphere of reciprocal space located a set of diffraction maxima with no systematic absences or symmetry, indicating a triclinic space group. Subsequent solution and refinement of the structure confirmed the centrosymmetric choice, $P\bar{1}$. Data were collected in the usual manner, using a continuous θ–2θ scan technique. Data were reduced in the usual manner. The structure was solved by a combination of Patterson and Fourier techniques. Hydrogen atoms were visible in a Fourier phased on the non-

hydrogen parameters and were included in the final cycles. Non-hydrogen atoms were assigned anisotropic thermal parameters while hydrogens were allowed to vary isotropically. A final difference Fourier was essentially featureless, with the largest peak being 0.40 e/Å³.

Registry No. W₂Bz₂(O₂CEt)₄, 91585-90-9; W₂Bz₂(O₂CMe)₄, 110142-67-1; W₂Bz₂(O₂CH)₄, 110142-68-2; W₂Bz₂(O₂CCMe₃)₄, 110142-69-3; W₂Bz₂(O₂CPh)₄, 110142-70-6; W₂(o-MeC₆H₄)₂(O₂CEt)₄, 110142-71-7; W₂(p-MeC₆H₄)₂(O₂CEt)₄, 110173-56-3; W₂Me₂(O₂CPh)₄, 110142-72-8; W₂Me₂(O₂CMe)₄, 110142-73-9; W₂(CH₂CHMe₂)₂-(O₂CMe)₄, 110142-74-0; W₂(CH₂CHMe₂)₂(O₂CPh)₄, 110173-57-4; W₂(CH₂SiMe₃)₂(O₂CMe)₄, 110142-75-1; W₂(np)₂(O₂CH)₄, 110142-76-2; W₂(np)₂(O₂CMe)₄, 108603-67-4; W₂(np)₂(O₂CEt)₄, 91549-47-2; W₂(np)₂(O₂CCMe₃)₄, 110142-77-3; W₂(np)₂(OAc)₃(TFA), 110142-78-4; W₂(np)₂(OAc)₂(TFA)₂, 110142-79-5; W₂(np)₂(OAc)(TFA)₃, 110142-80-8; W₂(np)₂(TFA)₄, 110142-81-9; W₂(np)₂(O₂CPh)₄, 110142-82-0; W₂(np)₂(O₂CC₆H₄-p-OMe)₄, 110142-83-1; W₂(np)₂-(O₂CCHPh₂)₄, 110142-84-2; W₂(np)₂(O₂C-mesityl)₄, 110142-85-3; Mo₂(np)₂(O₂CMe)₄, 108581-85-7; W₂Bz₂(NMe₂)₄, 82555-52-0; W₂Bz₂(O-i-Pr)₄, 99639-27-7; W₂(np)₂(NMe₂)₄, 72286-69-2; W₂(np)₆, 54453-68-8; W₂(O₂CCF₃)₄, 77479-85-7; W₂(np)₂(O-i-Pr)₄, 101860-13-3; W₂Me₂(NMe₂)₄, 72286-64-7; W₂(CH₂CHMe₂)₂(NMe₂)₄, 101860-16-6; W₂(CH₂SiMe₃)₂(NMe₂)₄, 72286-70-5; W₂(o-MeC₆H₄)₂(NMe₂)₄, 84417-27-6; W₂(p-MeC₆H₄)₂(NMe₂)₄, 84417-28-7; Mo₂(np)₂(NMe₂)₄, 72286-61-4; W₂Et₂(NMe₂)₄, 72286-65-8; W₂(O₂CEt)₄, 88921-51-1; W₂(O₂CPh)₄, 110173-58-5; W₂(O₂C-p-MeOC₆H₄)₄, 110142-86-4; W₂-(O₂CH)₄, 96482-79-0; Ph₂CHCO₂H, 117-34-0; propionic anhydride, 123-62-6; pivalic anhydride, 1538-75-6; benzoic anhydride, 93-97-0; p-methoxybenzoic anhydride, 794-94-5; mesitylbenzoic acid, 480-63-7; tungsten, 7440-33-7; molybdenum, 7439-98-7.

Supplementary Material Available: Anisotropic thermal parameters and complete listing of bond distances and angles for W₂(np)₂(O₂CEt)₄, W₂Bz₂(O₂CEt)₄, W₂(np)₂(O₂CPh)₄, W₂-(np)₂(O₂CH)₄, Mo₂(np)₂(O₂CMe)₄, and W₂(np)₂(O₂CMe)₂-(O₂CCF₃)₂ (19 pages); F_o and F_c values for the same compounds (63 pages). Ordering information is given on any current masthead page. The complete structure reports are available from the Indiana University Chemistry Library in microfiche form only at $2.50 per copy. Request MSC Report No. 84210 for W₂-(np)₂(O₂CEt)₄, 84005 for W₂Bz₂(O₂CEt)₄, 85022 for W₂(np)₂-(O₂CPh)₄, 85057 for W₂(np)₂(O₂CH)₄, 85132 for Mo₂(np)₂-(O₂CMe)₄, and 85055 for W₂(np)₂(O₂CMe)₂(O₂CCF₃)₂.